Electronic Supplementary Material (ESI) for ChemComm.

A New Class of Supramolecular Ligands Stabilizes 14-3-3 Protein-Protein Interactions by up to Two Orders of Magnitude

A. Gigante, J.-N. Grad, J. Briels, M. Bartel, D. Hoffmann, C. Ottmann, and C. Schmuck

Supporting Information

1. Protein expression and purification

Escherichia coli Rosetta (DE3) cells (Merck, Nottingham, England) transformed with the cloned vector were used to inoculate 50 mL Luria-Bertani (LB) medium containing ampicillin with a concentration of 100 mg/mL. The culture was grown for 12 h at 310 K with vigorous shaking. The pre-culture was used to inoculate a 5 L Terrific Broth (TB) culture containing 100 mg/mL ampicillin. The culture was shaken at 140 rpm at 310 K until an OD_{600} of 0.4-0.6 was reach. Protein expression was started by adding 0.4 mM IPTG to the culture. The culture was incubated at 298 K for 12 h and then harvested by centrifugation.

The bacterial pellet was re-suspended in buffer, containing 50 mM Tris-HCl, 300 mM NaCl, 5% glycerol, 10 mM imidazole, 0.5 mM TCEP and 1 mM PMSF pH 8.0. The cells were lysed, using a microfluidizer. The lysate was cleared and purified using an AKTA Purifier system (GE Healthcare, Freiburg, Germany) and Ni-NTA resin (GE Healthcare, Freiburg, Germany) according to the manufacturers' manuals. The resin was washed in buffer consisting of 50 mM Tris-HCl, 500 mM NaCl, 5% glycerol, 25 mM imidazole and 0.5 mM TCEP pH 8.0. The protein was eluted in buffer consisting of 50 mM HEPES, 200 mM NaCl, 5% glycerol, 250 mM imidazole, 0.5 mM TCEP pH8.0. The eluted protein was dialyzed against 25 mM HEPES, 100 mM NaCl, 10 mM $MgCl_2$, 1 mM β-mercaptoethanol, pH7. The 14-3-3 protein was then concentrated to 50 mg/mL. The protein was aliquoted, flash-frozen in liquid nitrogen, and stored at 193 K.

2. Fluorescence Polarization (FP) assays

The Fluorescence Polarization measurements were done on a filter-based microplate reader (Tecan Infinite F500). The FAM-labeled peptides were measured with an excitation wavelength of λ_{ex}: 485±20 nm and at an emission wavelength of λ_{em}: 535±25 nm. All measurements were done with an integration time of 50 µs in black, flat-bottom 384 microwell plates (Corning, # 4514/3676) and a buffer containing 10 mM HEPES, 150 mM NaCl, 0.1% (v/v) Tween 20 and 0.1% (m/v) BSA. The following labeled peptide sequences were used to test the stabilization effect of the multivalent peptides: (5-FAM)-RRKpSV (Task3), (5,6-FAM)-RTPpSLPTGGGSGGSGGGSKCGpSLGNIHHK (Tau) and (5-FAM)-RQRSTpSTPNVH (C-Raf). Both peptides were bought from Caslo, Denmark. GraphPad Prism 5.03 software was used for data analysis.

First a titration of 14-3-3ζ protein on the effectors was done in order to select an appropriate protein concentration for the subsequent stabilization experiments.

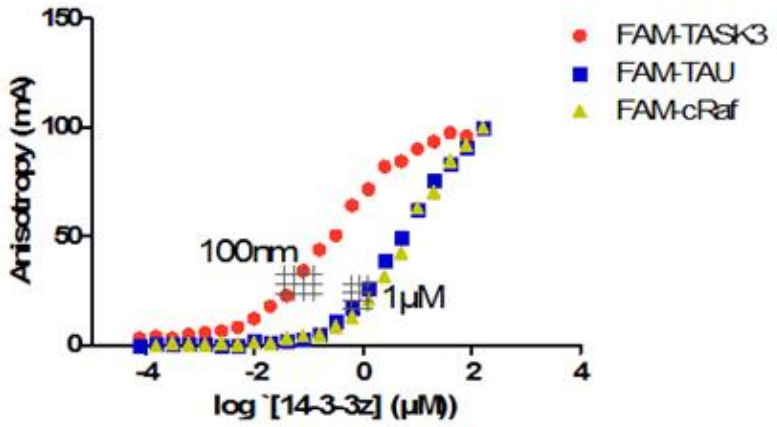

FigureS1. Direct binding of 14-3-3ζ and the protein partners (Task3, Tau and C-Raf).

Then, the multivalent compounds were titrated on the fluorescently labelled effectors (100 nM) and 14-3-3ζ at a fixed concentration (1 µM 14-3-3 protein concentration for the case of Tau and C-Raf effectors, while for Task3 100 nM of 14-3-3 protein was used) until saturation (normally used 1 mM ligand concentration). The measured anisotropy values were plotted against the logarithmic concentration of the compounds and the resulting curve was fitted to a four-parameter logistic model (4PL) to obtain the EC_{50} values.

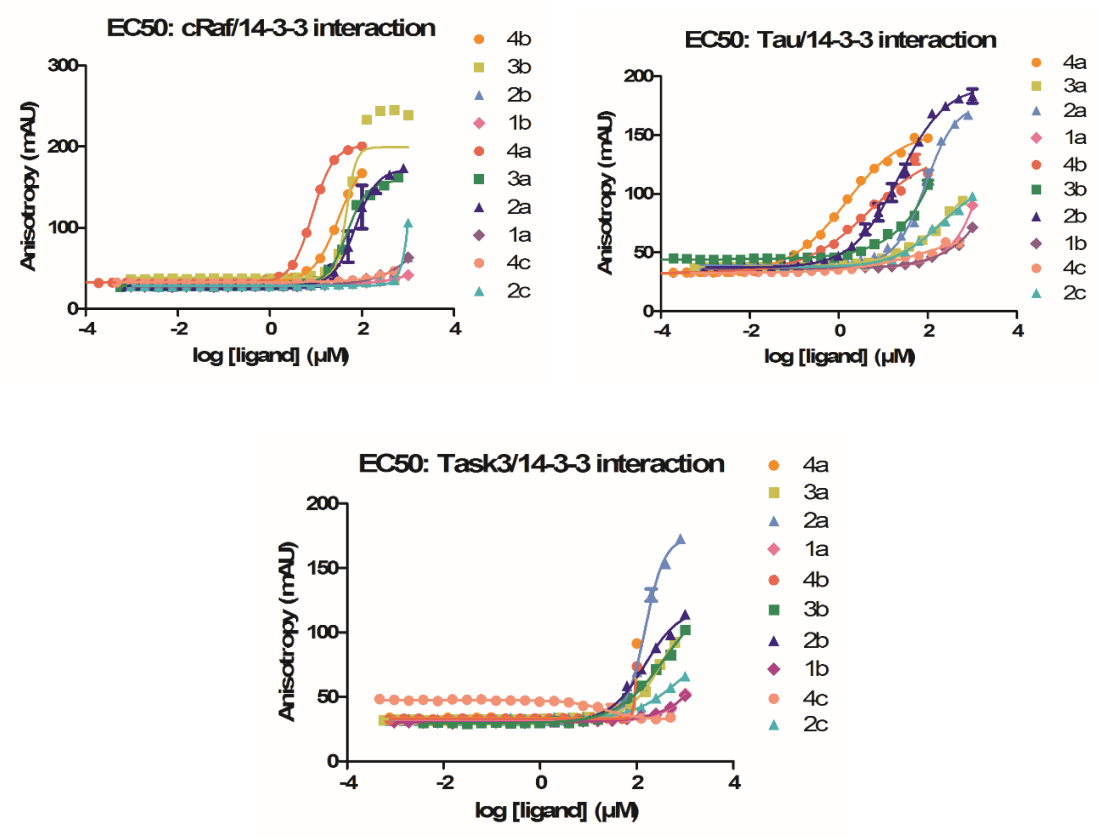

Figure S2. Curves of EC_{50} of 14-3-3ζ/effector (C-Raf, Tau and Task3) titrated with our ligands.

The same experiment was carried out for **4a** and **4b** in absence of the 14-3-3 protein. These ligands (1 mM) were titrated on the fluorescently labelled C-Raf and Tau effectors (100 nM). The measured anisotropy values were plotted against the logarithmic concentration of the compounds. The results indicate that these compounds do not bind to these effectors.

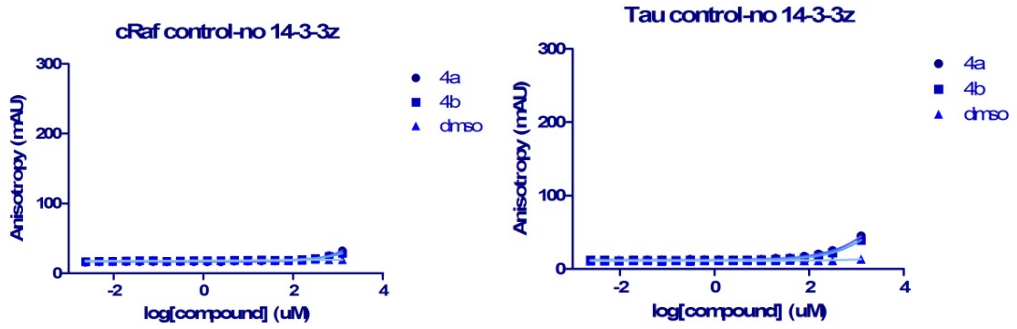

Figure S3. Control experiment: tritation of **4a** and **4b** on labelled C-Raf and Tau effectors.

For the determination of the K_D values a one site binding model ($y=[(B_{max}*x).(x+K_D)^{-1})]+nonspecific\ binding.x$) was used for fitting of the data. Thus, 14-3-3ζ (240 µM) was titrated on the fluorescently labelled effectors (100 nM) in the presence of 50 µM of the ligands.

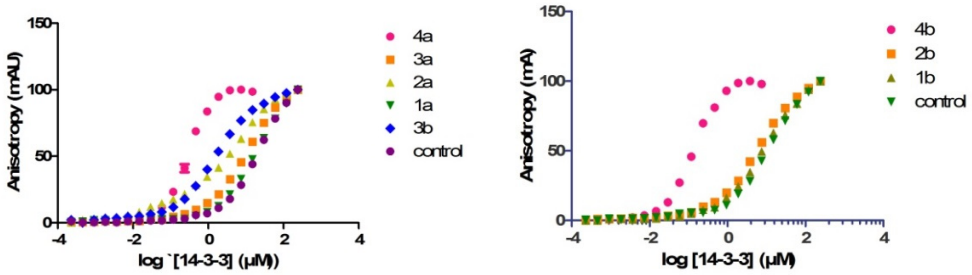

Figure S4. Apparent K_D of the 14-3-3ζ/C-Raf interaction in the presence of 50 µM of different ligands.

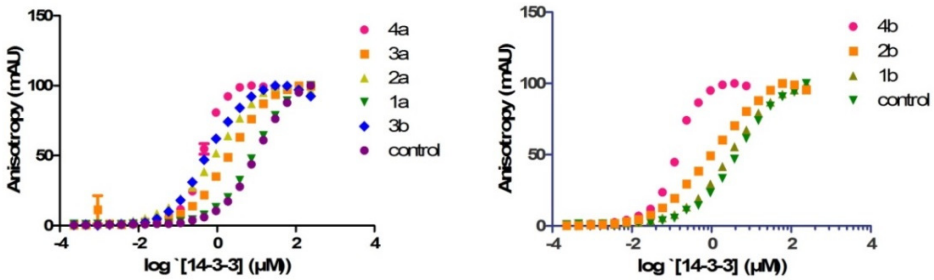

....

Figure S5. Apparent K_D of the 14-3-3ζ/Tau interaction in the presence of 50 µM of different ligands.

3. Isothermal Titration Calorimetry (ITC) measurements

Isothermal Titration Calorimetry (ITC) experiments were conducted on a MicroCal iTC2000 microcalorimeter (Malvern Instruments Ltd). The following unlabeled peptide sequences were used to test the stabilization effect of **4b** ligand: RQRSTpSTPNVH (Raf) and RTPpSLPTGGGSGGSGGGSKCGpSLGNIHHK (Tau). Origin 7.0 software, supplied by the manufacturer, was used for data acquisition and analysis.

All measurements were carried out in a buffer containing 25 mM HEPES pH 7.5, 100 mM NaCl, 2 mM $MgCl_2$ and 4 mM of 2-mercaptoethanol at 25 ºC. Aliquot of the effectors (4 µL, C-Raf at 1.5 mM and Tau at 2.5 mM) were injected from a 60 µL rotating syringe (750rpm) into the calorimeter reactor cell containing 300 µL of 60 µM 14-3-3ζ in the case of study the interaction with C-Raf and 100 µM of the protein for the Tau interaction. To measure the stabilizing potency of **4b** compound on both interactions: 14-3-3/C-Raf and 14-3-3/Tau, the sample cell was loaded with 25 µM 14-3-3ζ and 50 µM of this ligand. Then, the C-Raf or Tau peptide was titrated (4 µL) with 1.5 mM or 2.5 mM, respectively. Data were analysed according to a nonlinear least squares routine using a single-site binding model. Blank experiments were conducted to calculate the heats of dilution of C-Raf and Tau. These were subtracted from the heat measured in the titration experiments.

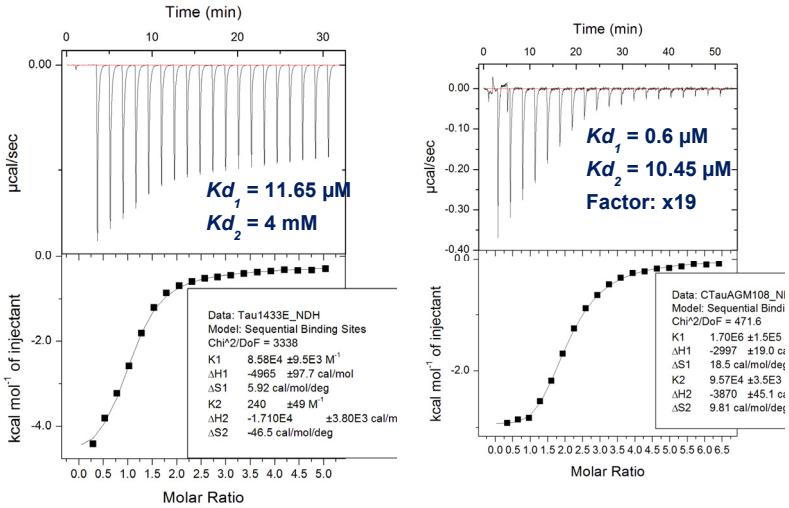

Figure S6. Isothermal titration calorimetry of binding Tau to 14-3-3ζ (A) and in the presence of 50 µM of 4b compound (B).

4. Microscale Thermophoresis (MST) experiments

For performing experiments with the 14-3-3ζ protein a fluorescent label (NT-647) was covalently attached to the protein (NHS coupling). In the MST experiment we kept the concentration of NT-647 labelled protein constant (100 nM), while the concentration of the ligands was varied between 100 µM – 6 nM. The assay was performed in a buffer (pH 7.5) containing 10 mM HEPES, 150 mM NaCl, 2 mM, $MgCl_2$ and 0.05% Tween20. After a short incubation the samples were loaded into the MST NT.115 standard glass capillaries and the MST analysis was performed using the Monolith NT115. Concentrations on the x-axis are plotted in nM.

A K_D (4b) = 5.1 ± 0.3 µM

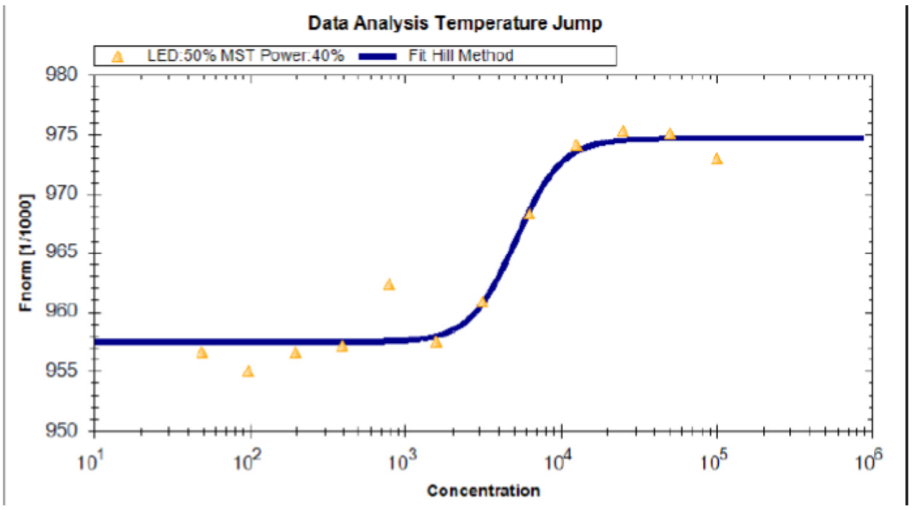

B K_D (4a) = 22 µM

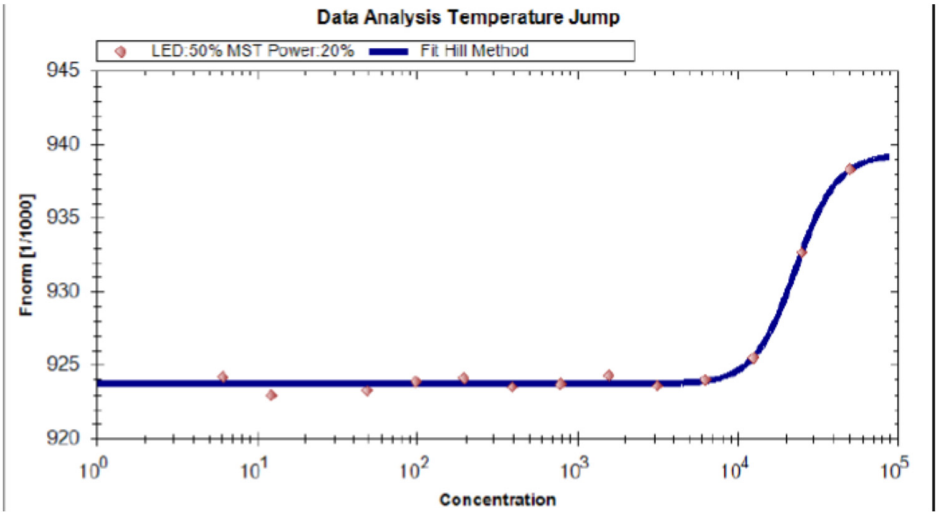

Figure S7. Dissociation constants (K_D) of **4b** (A), **4a** (B), **3a** (C) and **1a** (D) ligands.

C K_D (3a) = 41.0 ± 0.6 µM

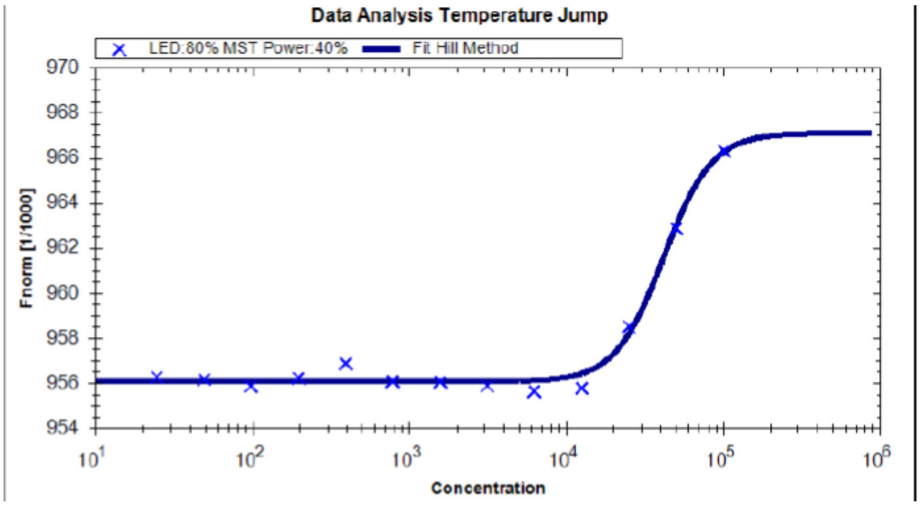

D K_D (1a) = No binding

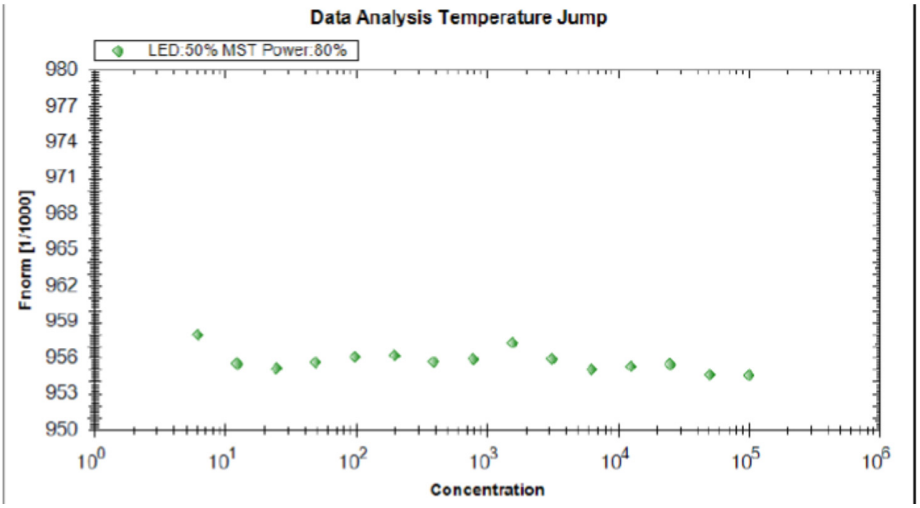

Figure S7. Dissociation constants (K_D) of **4b** (A), **4a** (B), **3a** (C) and **1a** (D) ligands.

5. Molecular Dynamics simulations (MDs)

MD simulations were carried out with Gromacs 4.6.7[1] using the methodology and parameters described in the literature.[2] 12 simulations were produced: a set of 6 pilot simulations of 30 ns to sample the binding event (Figures 3, 4, S8), followed by a set of 6 production simulations of 250 ns, amounting to 1.5 μs, for the statistical analysis of salt bridge formation (Figure S9). We determined the frequency of salt bridge formation between ligand **4b** and the 14-3-3/C-Raf receptor by measuring the N···O distance between their charged groups (Lys ε-ammonium group, GCP guanidinium group, Asp/Glu side-chain carboxylate groups, C-Raf peptide *C*-terminal carboxylate group) using a cutoff value of 3.2 Å. Figure S9A shows how often the 6 basic residues in ligand **4b** interacted with acidic groups from the 14-3-3ζ/C-Raf complex. Overall GCP formed salt bridges more frequently than Lys. Figure S9B shows that in MD 2, 3, and 6 the third arm did not actively participate in salt bridge formation.

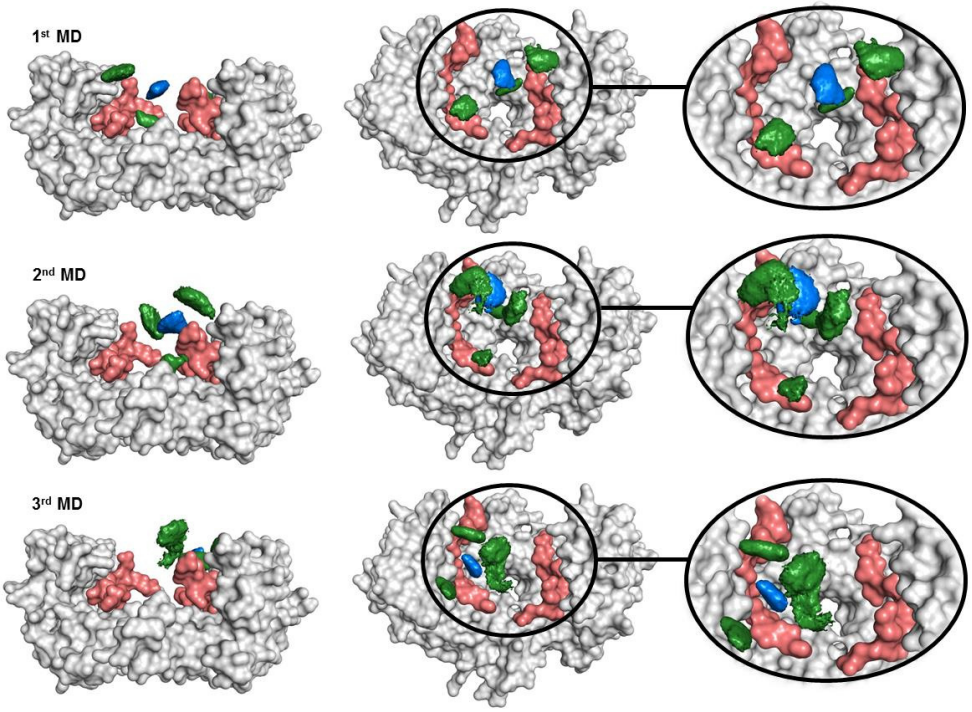

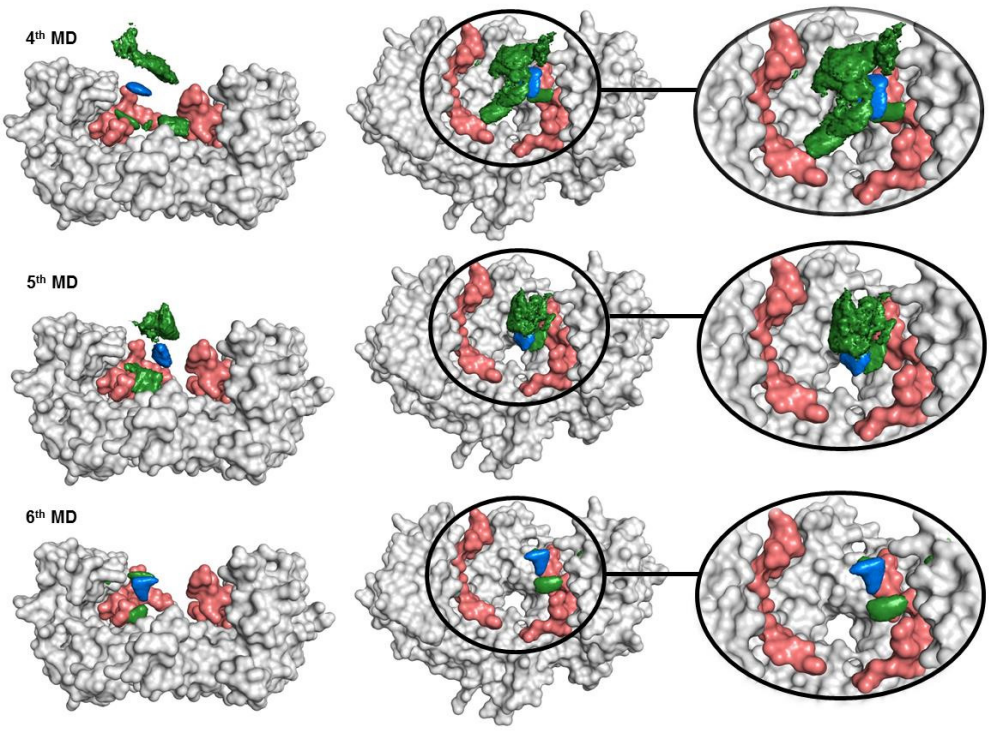

Figure S8. Six MD simulations of 14-3-3ζ dimer (grey) with C-Raf peptides (salmon) and peptidic arms containing GCP (green) as well as the central benzene ring (blue). Green and blue volumes indicate presence in at least 25% of the MD trajectories.

A

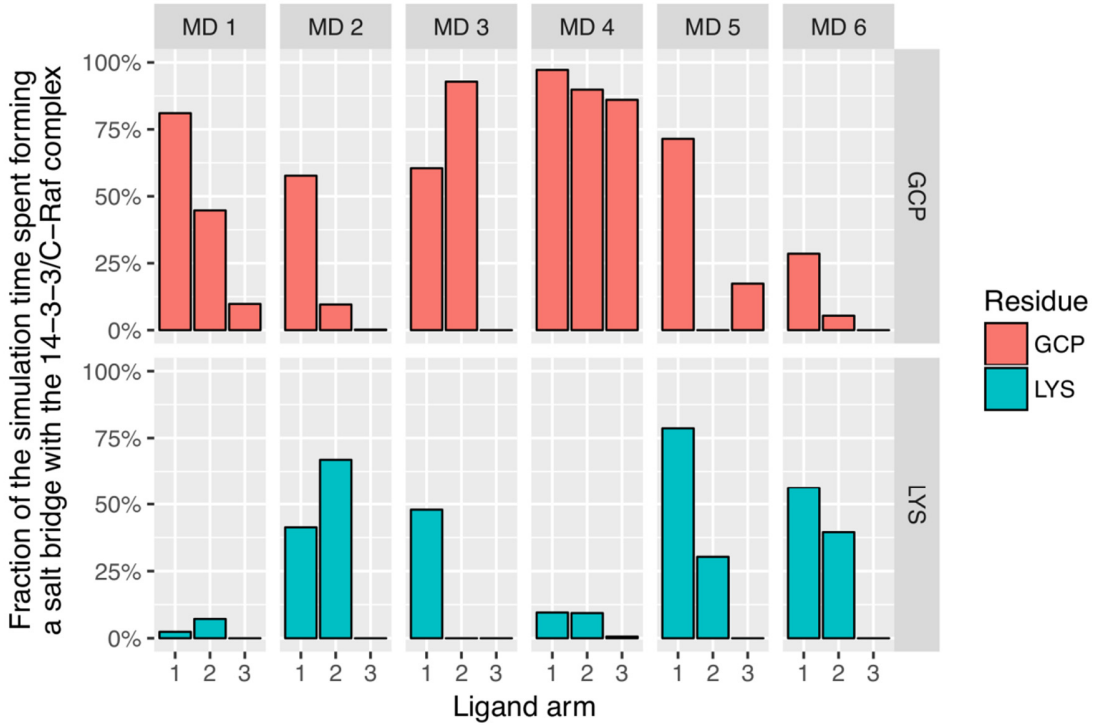

B

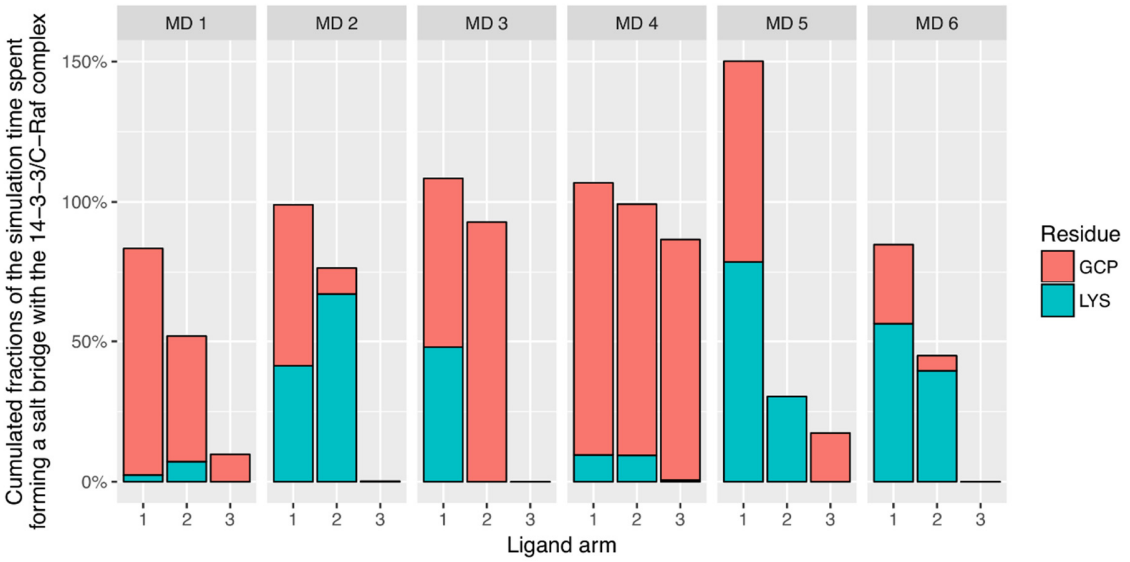

Figure S9. Salt bridge frequency in the MD simulations involving the 14-3-3/C-Raf/**4b** complex. (A) The three chemically equivalent arms in ligand **4b** are labeled 1, 2, and 3 by decreasing frequency of binding. (B) combines the same results from (A) in one graphic to highlight the relative contribution of each arm.

6. Chemistry

a. General Remarks

Solvents were dried and distilled before use. Millipore water was obtained with a Micropure from TKA. All reactions were carried out in oven dried glassware. Microwave assisted SPPS was carried out with a CEM Discover. Analytical TLC was carried out on SiO_2 aluminum foils ALUGRAM SIL G/UV254 from Macherey Nagel. The analytical "High Performance Liquid Chromatography" (HPLC) was done with Dionex HPLC apparatus: P680 pump, ASI-100 automated sample injector, UVD-340U UV detector, UltiMate 3000 Column Compartment. Commercially available HPLC grade solvents were used as eluents and solvent mixtures are reported in volume percent. Lyophilization was carried out with an Alpha 1-4 2D plus freeze drying apparatus from Christ. Reversed phase column chromatography was done with an Armen Instrument Spot Flash Liquid Chromatography MPLC apparatus with RediSep C-18 Reversed-Phase columns. ^{1}H- and 13C-NMR spectra were recorded on a Brucker DRX 500 MHz and Bruker Avance 700 spectrometer at ambient temperature. The chemical shifts are reported in parts per million (ppm) relative to the deuterated solvent DMSO-d6. The following abbreviations are used for peak multiplicities: s, singlet; d, doublet; m, multiplet; br, broad. High resolution ESI mass spectra were recorded with a Bruker BioTOF III spectrometer. Melting points were measured in open glass capillary tubes with a Büchi Melting Point B-540 instrument and are quoted uncorrected. Determination of pH values was carried out with a pH-Meter766 Calimatic from Knick.

b. Synthesis and characterization

Compounds **1a**, **1b**, **2a**, **2c**, **4a**, **4b** and **4c** were synthesized as is described in the literature.[3]

Synthesis of the acyl hydrazone 2b: to a microwave vial containing benzene-1,4-dialdehide (2.60 mg, 19.38 µmol) in 2 mL of MeOH, **1b** (34.49 mg, 42.64 µmol) was added. Then, the mixture was heated microwaved irradiated at 60 ºC for 1h. After the solvent was removed, the crude was purified by RP18-MPLC using appropriate conditions (MeOH/H_2O + 0.005% TFA) to obtain 18 mg (54%) of **2b** as a white solid. HPLC purity: 98%. ^{1}H-NMR (500 MHz, DMSO-*d6*): *δ* (ppm) 1.17-1.31 (m, 8H, 4 x Lys-CH_2), 1.40-1.70 (m, 16H, 8 x Lys-CH_2), 2.72- 2.78 (m, 4H, 2 x Lys-CH_2), 2.82-2.93 (m, 2H, Trp-CH_2), 2.97-3.03 (m, 2H, Trp-CH_2), 3.16-3.19 (m, 4H, 2 x Lys-CH_2), 3.71 (s, 4H, 2 x Gly-CH_2), 4.12-4.19 (m, 4H, 4 x Lys-CH), 4.45-4.48 (m, 2H, 2 x Trp-CH), 6.85-6.86 (m, 2H, 2 x GCP-CH_{ar}), 6.93-6.97 (m, 2H, 2

x Trp-CH_{ar}), 7.02-7.05 (m, 2H, Trp-CH_{ar}), 7.09 (s, 2H, NH_2), 7.12-7.18 (m, 4H, 2 x Trp-NH, 2 x GCP-CH_{ar}), 7.29-7.32 (m, 2H, Trp-CH_{ar}), 7.53-7.58 (m, 2H, Trp-CH_{ar}), 7.64-7-73 (m, 8H, 2 x Lys-NH_2, 4 x Phe-CH_{ar}), 7.78-7.83 (m, 2H, Lys-NH), 7.95-8.02 (m, 4H, 2 x Lys-NH, 2 x Trp-NH), 8.07 (s, 2H, 2 x Lys-NH), 8.10-8.12 (m, 2H, 2 x NH), 8.25 (s, 1H, Gly-NH), 8.30 (m, 2H, 2 x CH=N), 8.37 (s, 2H, NH), 8.44 (s, 2H, 2 xNH), 8.50 (s, 2H, NH), 10.81 (s, 2H, 2 x Trp-NH), 11.32 (s, 1H, NH),11.55 (d, *J* = 11.4 Hz, 1H, NH), 12.34 (s, 2H, GCP-NH). ^{13}C-NMR (500 MHz, DMSO-*d6*): *δ* (ppm) 22.2 (Lys-CH_2), 22.9 (Lys-CH_2), 26.7 (Lys-CH_2), 27.1 (Lys-CH_2), 27.5 (Trp-CH_2), 28.8 (Lys-CH_2), 29.3 (CH_2), 29.9 (CH_2), 31.3 (Lys-CH_2), 31.3 (Lys-CH_2), 38.7 (Lys-CH_2), 42.2 (Gly-CH_2), 42.4 (Gly-CH_2), 52.3 (Lys-CH), 52.3 (Lys-CH), 53.7 (Trp-CH), 53.8 (Trp-CH), 109.9 (Trp-Cq), 111.3 (Trp-CH_{ar}), 112.3 (GCP-CH_{ar}), 115.4 (GCP-CH_{ar}), 118.1 (Trp-CH_{ar}), 118.3 (Trp-CH_{ar}), 120.9 (Trp-CH_{ar}), 123.6 (Trp-CH_{ar}), 125.4 (GCP-Cq), 127.0 (Phe-CH_{ar}), 127.2 (Trp-Cq), 129.0 (Phe-CH_{ar}), 132.8 (GCP-Cq), 135.4 (Phe-Cq), 136.1 (Trp-Cq), 142.2 (CH=NH), 155.1 (Gua-Cq), 158.1 (CO), 158.3 (CO), 159.1 (CO), 168.3 (CO), 169.6 (CO), 170.2 (CO), 171.2 (CO), 171.2 (CO), 171.8 (CO), 171.9 (CO), 172.4 (CO), 173.4 (CO), 173.7 (CO). LRMS (ESI): m/z calculated for $C_{80}H_{109}N_{28}O_{16}C_2F_3O_2H^{2+}$ $[M+C_2F_3O_2H+2H]^{2+}$: 915.9; found: 915.6.

Synthesis of the acyl hydrazone 3a: to a microwave vial containing benzene-1,3-dialdehide (2.00 mg, 14.91 µmol) in 2 mL of MeOH, **1a** (26.53 mg, 32.80 µmol) was added. Then, the mixture was heated microwaved irradiated at 60 ºC for 1h. After the solvent was removed, the crude was purified by RP18-MPLC using appropriate conditions (MeOH/H_2O + 0.005% TFA) to obtain 16 mg (62%) of **3a** as a white solid. HPLC purity: 96%. ^{1}H-NMR (500 MHz, DMSO-*d6*): *δ* (ppm) 1.22-1.29 (m, 8H, 4 x Lys-CH_2), 1.45-1.57 (m, 12H, 6 x Lys-CH_2), 1.59-1.71 (m, 4H, 2 x Lys-CH_2), 2.69- 2.75 (m, 4H, 2 x Lys-CH_2), 2.88-2.91 (m, 2H, Trp-CH_2), 2.96-3.01 (m, 2H, Trp-CH_2), 3.20-3.23 (m, 4H, 2 x Lys-CH_2), 3.69-3.73 (m, 4H, 2 x Gly-CH_2), 4.14-4.23 (m, 4H, 4 x Lys-CH), 4.48-4.51 (m, 2H, 2 x Trp-CH), 6.85 (s, 2H, 2 x GCP-CH_{ar}), 6.93-6.97 (d, *J* = 7.9 Hz, 2H, 2 x Trp-CH_{ar}), 7.04 (m, 4H, Trp-CH_{ar}, GCP-CH_{ar}) 7.08 (s, 2H, NH_2), 7.14 (s, 2H, Trp-NH), 7.19-7.21 (m, 2H, Trp-CH_{ar}), 7.29-7.32 (m, 2H, Trp-CH_{ar}), 7.53-7.56 (m, 2H, Trp-CH_{ar}), 7.64-7-73 (m, 8H, 2 x Lys-NH_2, 4 x Phe-CH_{ar}), 7.77-7.80 (m, 2H, Lys-NH), 7.98-8.05 (m, 4H, 2 x Lys-NH, 2 x Trp-NH), 8.21 (s, 1H, Gly-NH), 8.34 (s, 2H, CH=N), 8.43 (s, 2H, 2 x NH), 10.79 (s, 2H, 2 x Trp-NH), 11.22 (s, 2H, 2 x NH), 11.31 (d, *J* = 17.1 Hz, 1H, NH),11.50 (d, *J* = 11.4 Hz, 1H, NH), 12.32 (s, 2H, GCP-NH). ^{13}C-NMR (500 MHz, DMSO-*d6*): *δ* (ppm) 22.1 (Lys-CH_2), 22.8 (Lys-CH_2), 26.6 (Lys-CH_2), 27.2 (Lys-CH_2), 27.5 (Trp-CH_2), 28.8 (Lys-CH_2), 29.3 (CH_2), 29.4 (CH_2), 30.0 (CH_2), 31.0 (Lys-CH_2), 31.7

(Lys-CH_2), 38.7 (Lys-CH_2), 38.8 (Lys-CH_2), 42.2 (Gly-CH_2), 42.3 (Gly-CH_2), 52.4 (Lys-CH), 52.4 (Lys-CH), 52.5 (Lys-CH), 53.7 (Trp-CH), 53.7 (Trp-CH), 109.9 (Trp-Cq), 111.3 (Trp-CH_{ar}), 112.3 (GCP-CH_{ar}), 115.3 (GCP-CH_{ar}), 118.2 (Trp-CH_{ar}), 118.3 (Trp-CH_{ar}), 120.8 (Trp-CH_{ar}), 123.6 (Trp-CH_{ar}), 123.6 (Phe-CH_{ar}), 127.2 (GCP-Cq), 127.2 (Trp-Cq), 129.2 (Phe-CH_{ar}), 132.8 (GCP-Cq), 134.4 (Phe-Cq), 136.0 (Trp-Cq), 142.2 (CH=NH), 155.1 (Gua-Cq), 157.8 (CO) 159.0 (CO), 159.6 (CO), 168.2 (CO), 169.4 (CO), 171.0 (CO), 171.1 (CO), 171.8 (CO), 171.9 (CO), 172.2 (CO), 172.2 (CO), 173.4 (CO), 173.6 (CO), 173.6 (CO). LRMS (ESI): m/z calculated for $C_{80}H_{109}N_{28}O_{16}C_2F_3O_2H^{2+}$ $[M+C_2F_3O_2H+2H]^{2+}$: 915.9; found: 915.6.

Synthesis of the acyl hydrazone 3b: to a microwave vial containing benzene-1,4-dialdehide (1.50 mg, 11.18 µmol) in 2 mL of MeOH, **1b** (19.00 mg, 24.60 µmol) was added. Then, the mixture was heated microwaved irradiated at 60 ºC for 1h. After the solvent was removed, the crude was purified by RP18-MPLC using appropriate conditions (MeOH/H_2O + 0.005% TFA) to obtain 11 mg (57%) of **2b** as a white solid. HPLC purity: 94%. ^{1}H-NMR (500 MHz, DMSO-*d6*): *δ* (ppm) 1.19-1.32 (m, 8H, 4 x Lys-CH_2), 1.39-1.71 (m, 16H, 8 x Lys-CH_2), 2.70- 2.78 (m, 4H, 2 x Lys-CH_2), 2.84-2.94 (m, 2H, Trp-CH_2), 2.95-3.04 (m, 2H, Trp-CH_2), 3.12-3.20 (m, 4H, 2 x Lys-CH_2), 3.72 (s, 4H, 2 x Gly-CH_2), 4.10-4.22 (m, 4H, 4 x Lys-CH), 4.43 (m, 2H, 2 x Trp-CH), 6.85 (m, 2H, 2 x GCP-CH_{ar}), 6.93-6.97 (m, 2H, 2 x Trp-CH_{ar}), 7.01-7.06 (m, 2H, NH_2), 7.07-7.13 (s, 2H, 2 x Trp-$H_{ar,}$ NH_2), 7.13-7.21 (m, 4H, 2 x Trp-NH, 2 x GCP-CH_{ar}), 7.29-7.32 (m, 2H, Trp-CH_{ar}), 7.53-7.56 (m, 2H, Trp-CH_{ar}), 7.62-7-75 (m, 6H, Lys-NH_2, 4 x Phe-CH_{ar}), 7.77-7.84 (m, 2H, 2 x Lys-NH), 7.95-8.02 (m, 4H, 2 x Lys-NH, 2 x Trp-NH), 8.03-8.09 (m, 2H, 2 x Lys-NH), 8.13-8.17 (m, 2H, 2 x NH), 8.23-8.29 (m, 2H, Gly-NH), 8.35 (s, 2H, 2 x CH=N), 8.44 (s, 2H, 2 x NH), 8.50 (s, 2H, 2 x NH), 10.81 (s, 2H, 2 x Trp-NH), 11.26 (s, 2H, 2 x NH), 11.31-11.34 (d, 1H, NH),11.54 (d, *J* = 11.4 Hz, 1H, NH), 12.34 (s, 2H, GCP-NH). ^{13}C-NMR (500 MHz, DMSO-*d6*): *δ* (ppm) 22.2 (Lys-CH_2), 22.9 (Lys-CH_2), 26.7 (Lys-CH_2), 27.1 (Lys-CH_2), 27.5 (Trp-CH_2), 28.8 (Lys-CH_2), 29.3 (CH_2), 30.0 (CH_2), 31.3 (Lys-CH_2), 31.3 (Lys-CH_2), 38.8 (Lys-CH_2), 42.3 (Gly-CH_2), 42.4 (Gly-CH_2), 52.3 (Lys-CH), 53.0 (Lys-CH), 53.7 (Trp-CH), 53.7 (Trp-CH), 109.9 (Trp-Cq), 111.3 (Trp-CH_{ar}), 112.3 (GCP-CH_{ar}), 115.4 (GCP-CH_{ar}), 118.0 (Trp-CH_{ar}), 118.3 (Trp-CH_{ar}), 120.9 (Trp-CH_{ar}), 123.7 (Trp-CH_{ar}), 125.4 (GCP-Cq), 126.9 (Phe-CH_{ar}), 127.2 (Trp-Cq), 129.1 (Phe-CH_{ar}), 132.8 (GCP-Cq), 135.4 (Phe-Cq), 136.0 (Trp-Cq), 142.2 (CH=NH), 155.1 (Gua-Cq), 158.1 (CO), 158.3 (CO), 159.0 (CO), 169.0 (CO), 169.6 (CO), 170.2 (CO), 171.2 (CO), 171.8 (CO), 172.4 (CO), 172.8 (CO), 173.4 (CO). LRMS (ESI): m/z calculated for $C_{80}H_{109}N_{28}O_{16}C_2F_3O_2H^{2+}$ $[M+C_2F_3O_2H+2H]^{2+}$: 915.9; found: 915.6

c. ^{1}H- and ^{13}C-NMR spectra

Compound 2b:

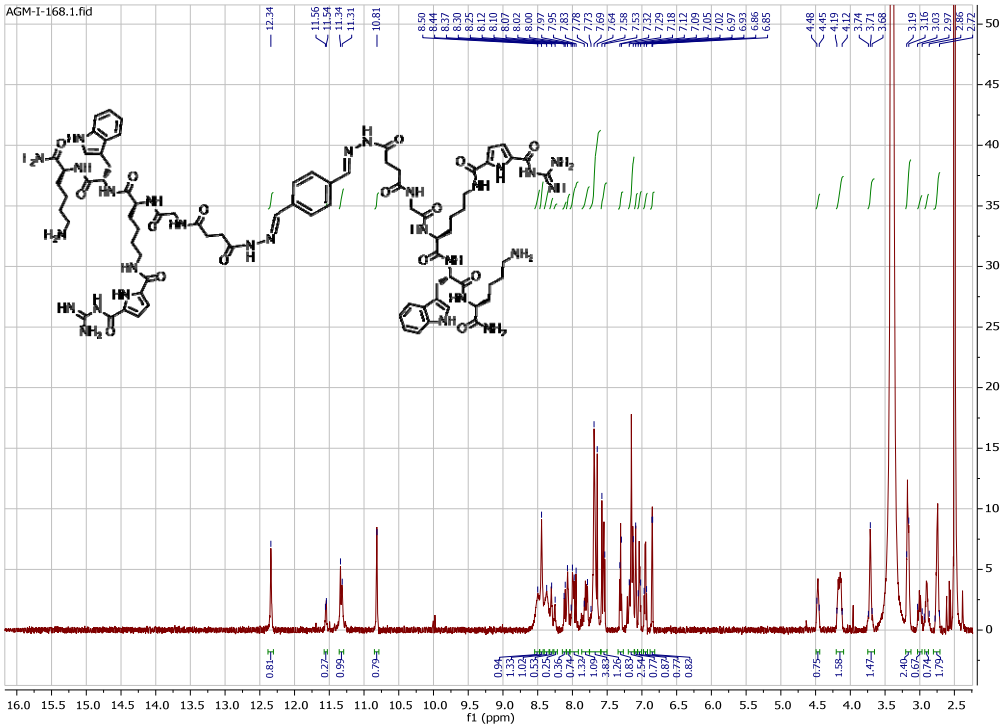

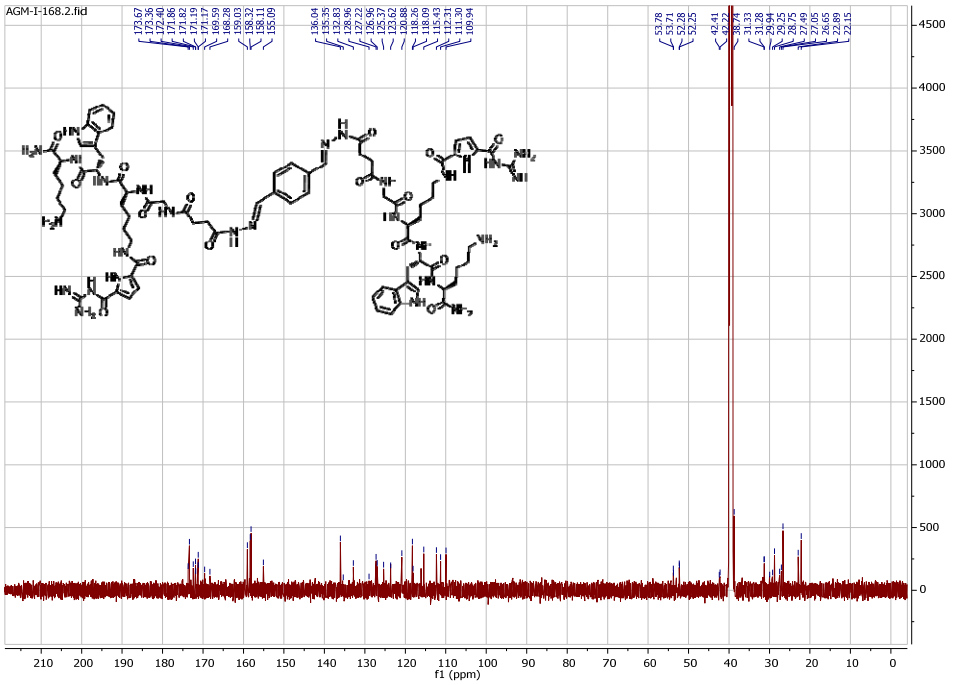

Compound 3a:

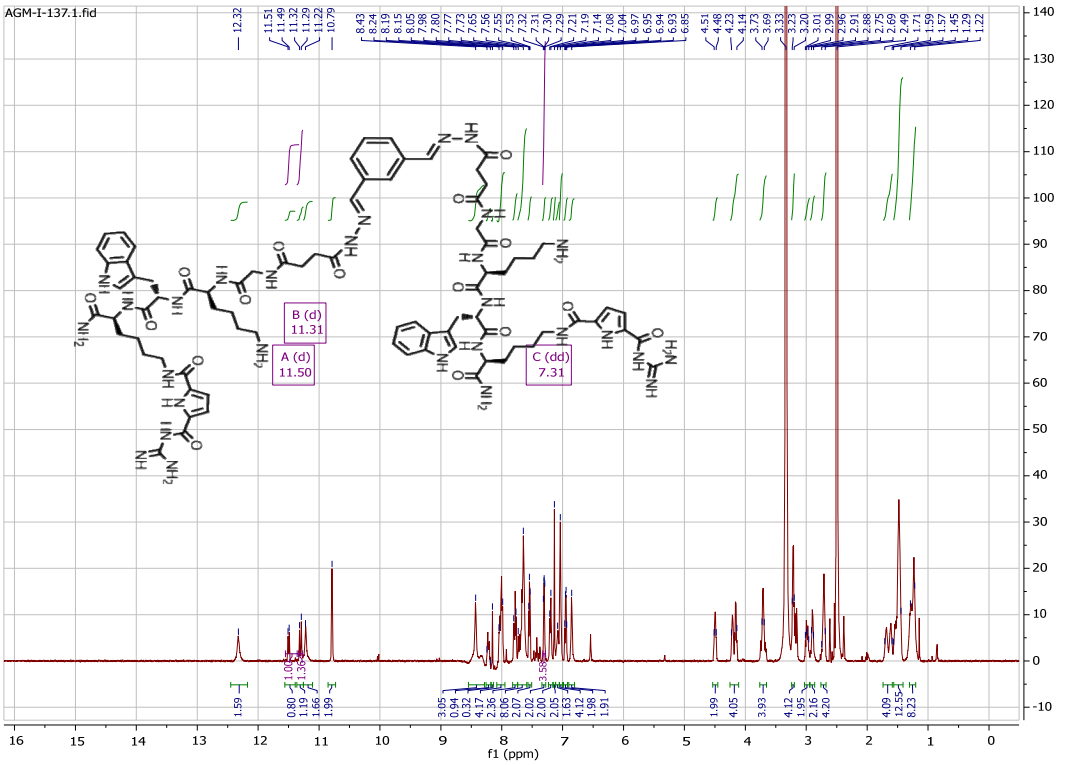
AGM-I-137.1.fid
B (d)
11.31
A (d)
11.50
C (dd)
7.31
f1 (ppm)

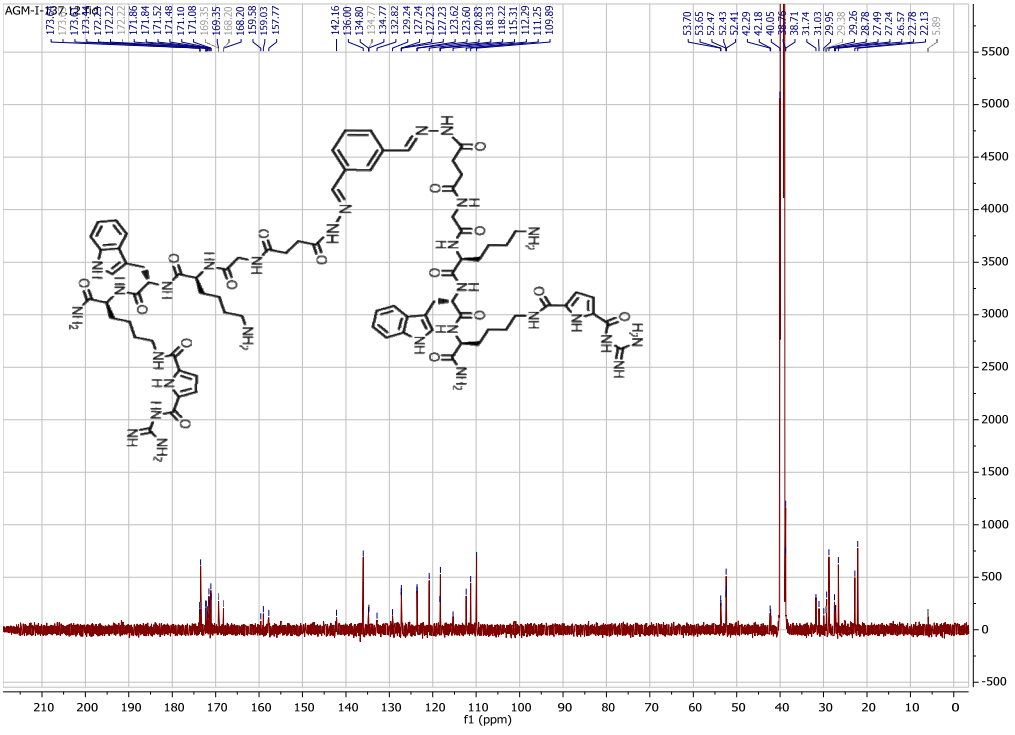
AGM-I-137.12.fid
f1 (ppm)

Compound 3b:

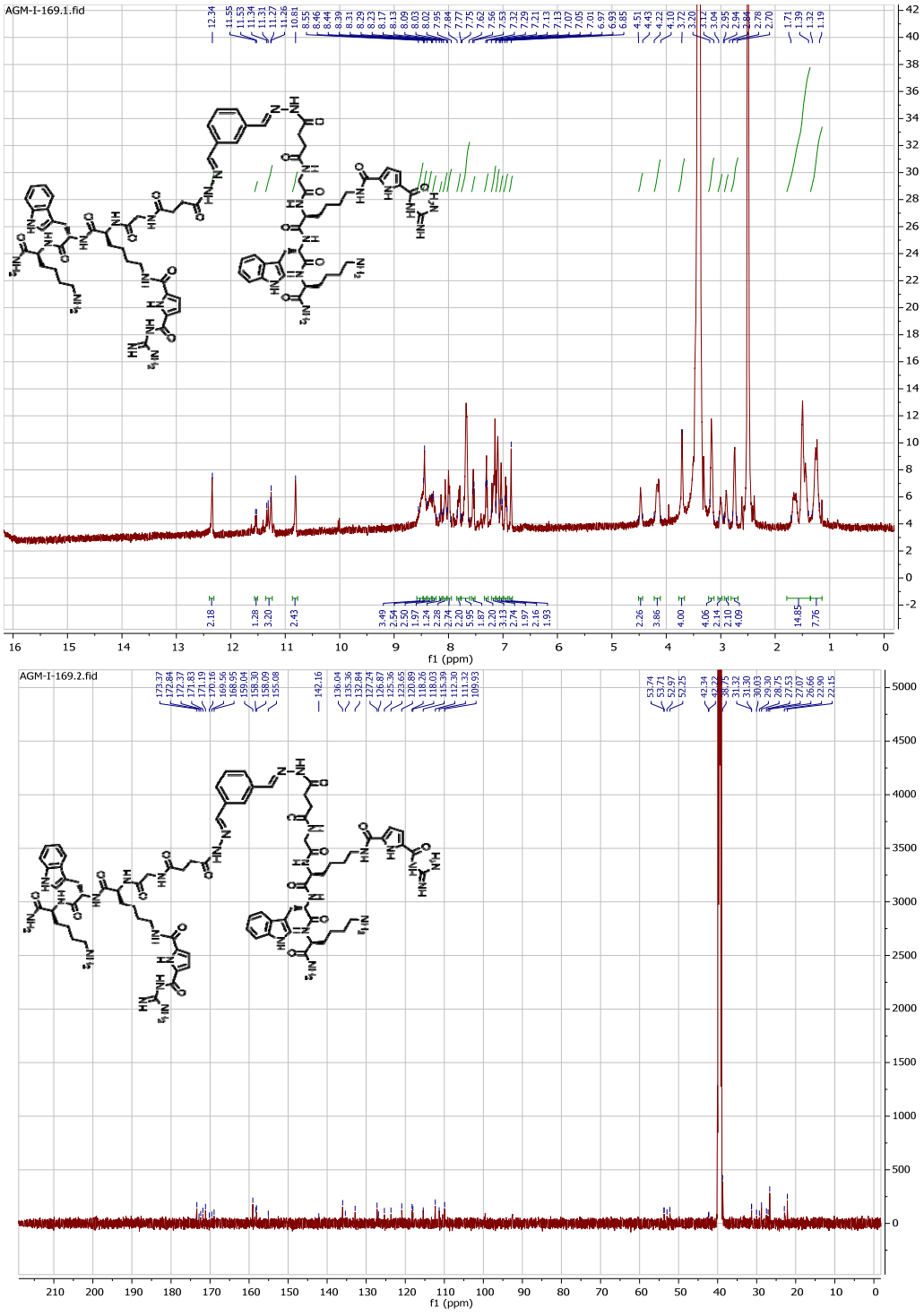

d. MS

Compound 2b:

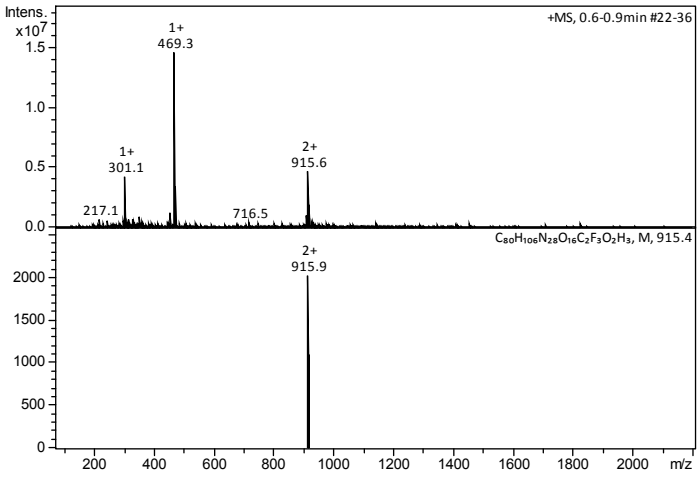

Compound 3a:

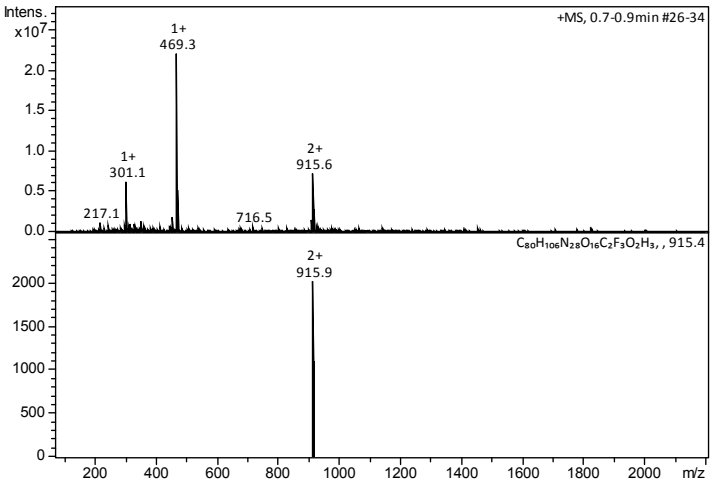

Compound 3b:

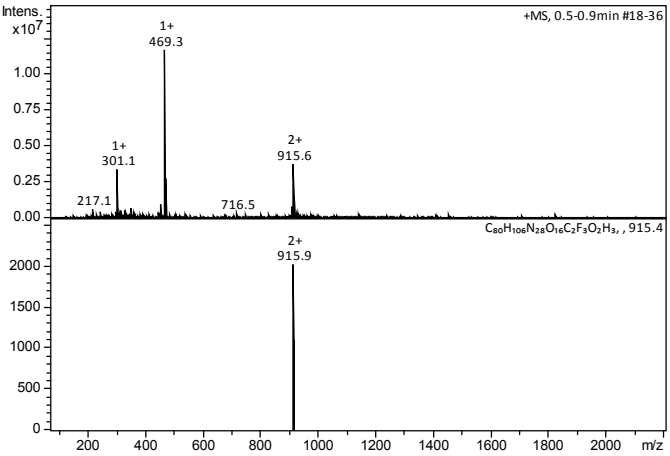

e. Purity by HPLC

Compound 2b:

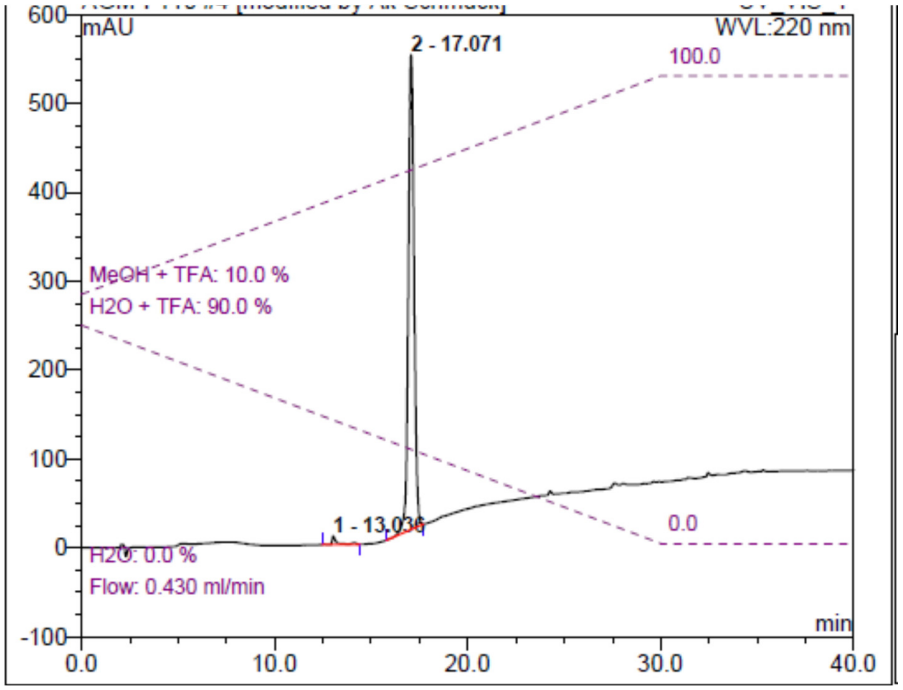

No.	Ret.Time min	Peak Name	Height mAU	Area mAU*min	Rel.Area %	Rel.Height %
1	13.04	n.a.	9.613	2.907	1.55	1.77
2	17.07	n.a.	533.719	184.161	98.45	98.23
Total:			*543.3319*	*187.07*	*100.00*	*100.00*

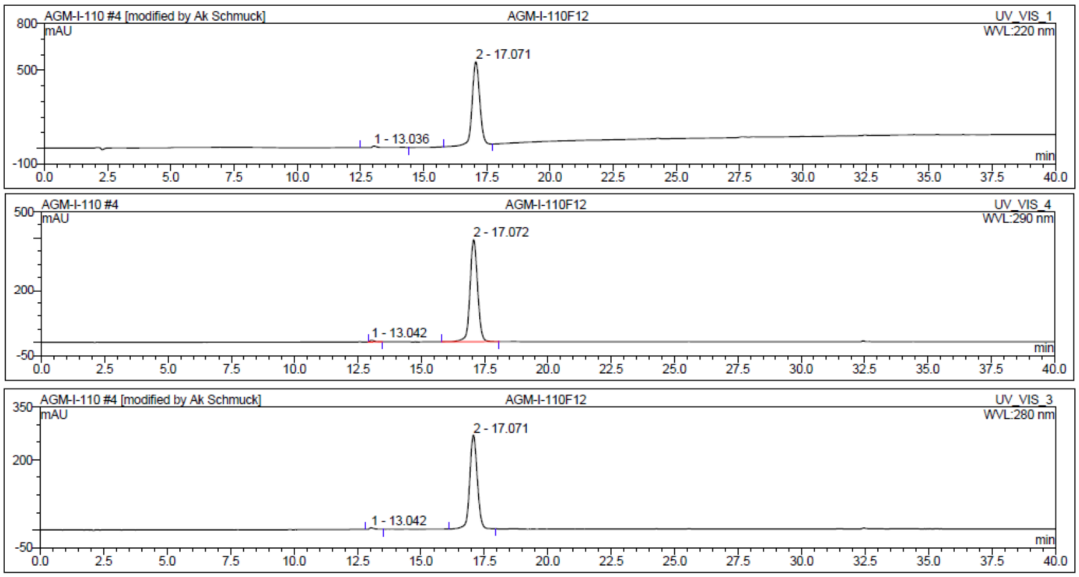

Compound 3a:

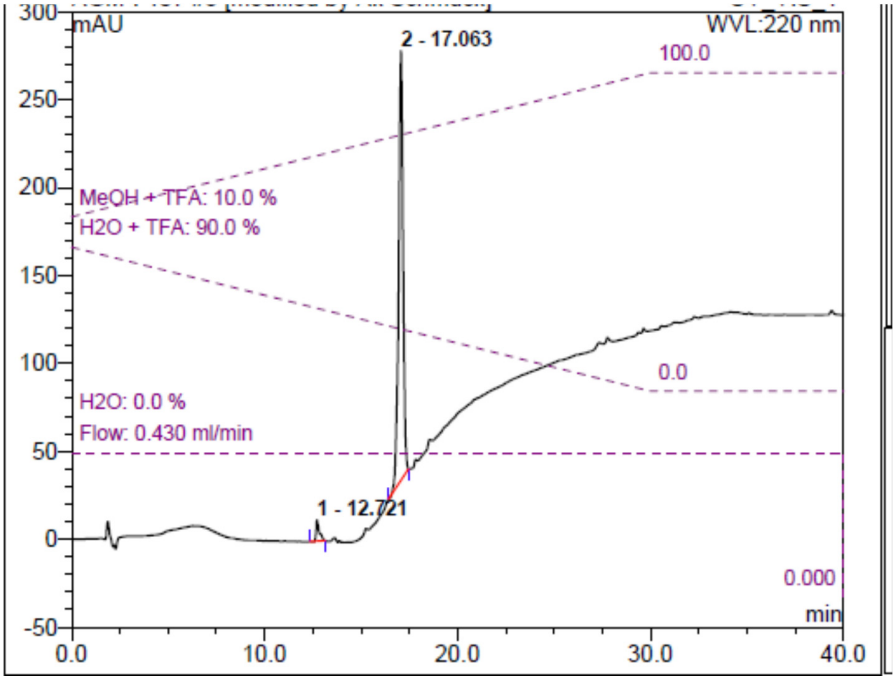

No.	Ret.Time min	Peak Name	Height mAU	Area mAU*min	Rel.Area %	Rel.Height %
1	12.72	n.a.	11.963	2.236	3.35	4.67
2	17.06	n.a.	244.122	64.578	96.65	95.33
Total:			*256.0851*	*66.81*	*100.00*	*100.00*

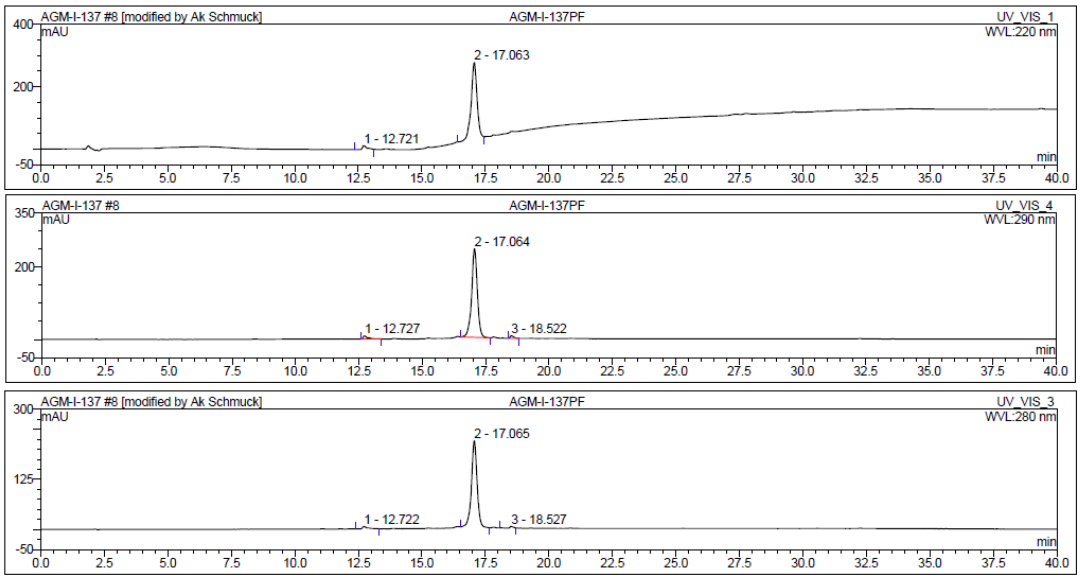

Compound 3b:

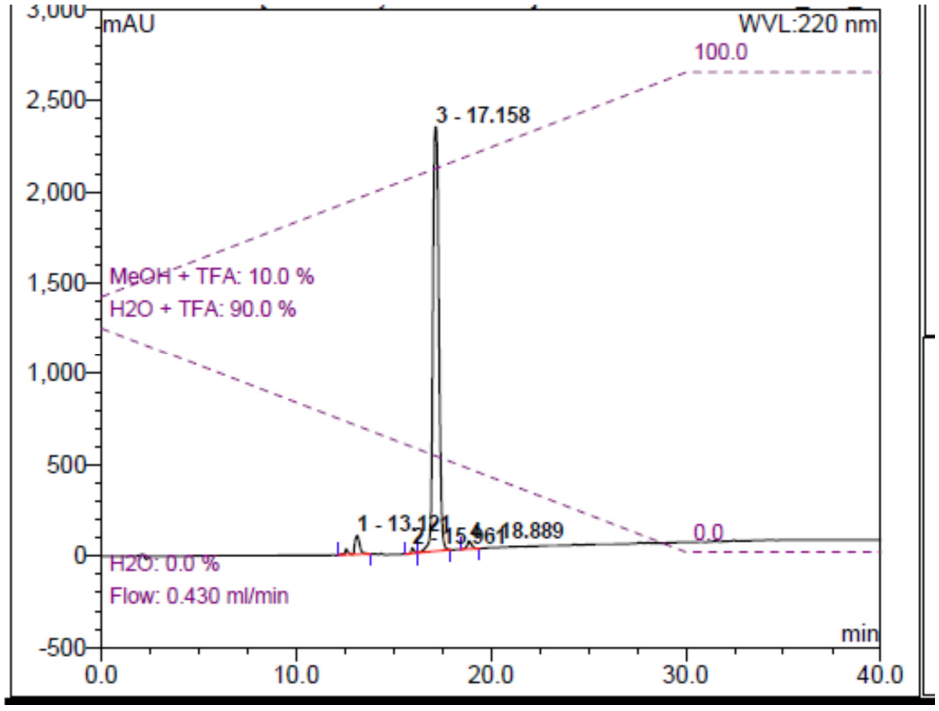

No.	Ret.Time min	Peak Name	Height mAU	Area mAU*min	Rel.Area %	Rel.Height %
1	13.12	n.a.	103.792	34.662	3.97	4.16
2	15.96	n.a.	28.520	4.418	0.51	1.14
3	17.16	n.a.	2327.355	822.946	94.31	93.23
4	18.89	n.a.	36.723	10.534	1.21	1.47
Total:			*2496.3905*	*872.56*	*100.00*	*100.00*

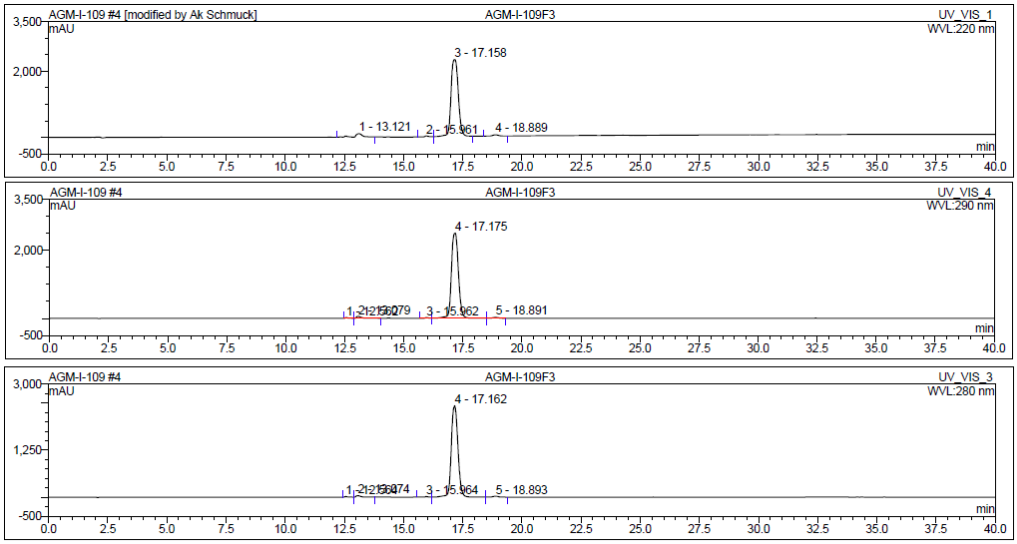

7. 14-3-3 crystal structures

Table S1: 14-3-3 crystal structures deposited in the PDB (November 2018).

PDB ID	Name	Resolution	Isoform	Organism	Ligand	Ref.
1A37	14-3-3ζ/C-RafpS259	3.60 Å	Zeta	Human	-	Liddington, RC et al. (1998) [1]
1A38	14-3-3ζ/R18	3.35 Å	Zeta	Human	-	Liddington, RC et al. (1998)[1]
1A4O	14-3-3ζ	2.80 Å	Zeta	Human	-	Liddington, RC et al. (1995)[2]
1QJA	14-3-3ζ/MODE2	2.00 Å	Zeta	Human	-	Yaffe, MB et al. (1999)[3]
1QJB	14-3-3ζ/MODE1	2.00 Å	Zeta	Human	-	Yaffe, MB et al. (1999)[3]
1IB1	14-3-3ζ/AANAT	2.60 Å	Zeta	Human	-	Dyda, F et al. (2001)[4]
1O9C	T14-3c	2.60 Å	Isoform c	Tobacco	Citrate	Oecking, C. et al. (2003)[5]
1O9D	T14-3c/PMA2pS955	2.30 Å	Isoform c	Tobacco	-	Oecking, C. et al. (2003)[5]
1O9E	T14-3c/FC-A	2.60 Å	Isoform c	Tobacco	Fusicoccin A	Oecking, C. et al. (2003)[5]
1O9F	T14-3c/PMA2pS955/FC-A	2.70 Å	Isoform c	Tobacco	Fusicoccin A	Oecking, C. et al. (2003)[5]
1YWT	14-3-3σ/MODE1	2.40 Å	Sigma	Human	-	Yaffe, MB. et al. (2005)[6]
1YZ5	14-3-3σ	2.80 Å	Sigma	Human	-	Hermeking, H. et al. (2005)[7]
2BQ0	14-3-3β	2.50 Å	Beta	Human	-	Doyle, DA. et al. (2006)[8]

2BR9	14-3-3ε/ConsPep	1.75 Å	Epsilon	Human	-	Doyle, DA. et al. (2006)[8]
2BTP	14-3-3τ/ConsPep	2.80 Å	Tau	Human	-	Doyle, DA. et al. (2006)[8]
2C23	14-3-3β/ExoS	2.65 Å	Beta	Human	-	Doyle, DA. et al. (2006)[8]
2C63	14-3-3η/ConsPep	2.15 Å	Eta	Human	-	Doyle, DA. et al. (2006)[8]
2C74	14-3-3 η/ConsPep	2.70 Å	Eta	Human	-	Doyle, DA. et al. (2006)[8]
2B05	14-3-3γ/MODE1	2.55 Å	Gamma	Human	-	-
2C1J	14-3-3ζ/H3pS10K9Ac	2.60 Å	Zeta	Human	-	Mahadevan, LC. et al. (2005)[9]
2C1N	14-3-3ζ/H3pS10	2.00 Å	Zeta	Human	-	Mahadevan, LC. et al. (2005)[9]
2NPM	14-3-3/ConsPep	2.52 Å		Cryptosporidium parvum	-	Hui, R. et al. (2011)[10]
2O8P	14-3-3/ConsPep	1.82 Å		Cryptosporidium parvum	-	Hui, R. et al. (2011)[10]
3EFZ	14-3-3/ConsPep	2.08 Å		Cryptosporidium parvum	-	Hui, R. et al. (2011)[10]
2O98	T14-3c/PMA2_CT52	2.70 Å	Isoform c	Tobacco	Fusicoccin A	Oecking, C. et al. (2007)[11]
2O02	14-3-3ζ/ExoS	1.50 Å	Zeta	Human/P. aeruginosa	-	Hallberg, B. et al. (2007)[12]
2V7D	14-3-3ζ/IntegBpT758	2.50 Å	Zeta	Human	-	Fagerholm, SC. et al. (2008)[13]
3E6Y	T14-3c/PMA2_pT955/CN-A	2.50 Å	Isoform c	Tobacco	Cotylenin A	Ottmann, C. et al. (2009)[14]
3CU8	14-3-3ζ/C-RafpS259	2.40 Å	Zeta	Human	-	Ottmann, C. et al. (2010)[15]
3LW1	14-3-3σ/p53pT387	1.28 Å	Sigma	Human	-	Ottmann, C. et al. (2010)[15]
3M50	T14-3e/PMA2_CT30/Epibestatin	2.60 Å	Isoform e	Nicotiana	Epibestatin	Ottmann, C. et al. (2010)[15]
3M51	T14-3e/PMA2_CT30/Pyrrolidone1	3.25 Å	Isoform e	Nicotiana	Pyrrolidone 1	Ottmann, C. et al. (2010)[15]
3IQJ	14-3-3σ/C-RafpS259 (10mer)	1.15 Å	Sigma	Human	-	Ottmann, C. et al. (2010)[15]
3IQU	14-3-3σ/C-RafpS259 (6mer)	1.05 Å	Sigma	Human	-	Ottmann, C. et al. (2010)[15]
3IQV	14-3-3σ/C-RafpS259 (6mer)/FC-A	1.20 Å	Sigma	Human	Fusicoccin A	Ottmann, C. et al. (2010)[15]
2WH0	14-3-3ζ/PKCpS346pS368	2.25 Å	Zeta	Human	-	McDonald, NQ. et al. (2009)[16]
3MHR	14-3-3σ/YAPpS127	1.15 Å	Sigma	Human	-	Ottmann, C. et al. (2010)[17]

3NKX	14-3-3ζ/C-RafpS259	2.40 Å	Zeta	Human	-	Ottmann, C. et al. (2010)[18]
3O8I	14-3-3σ/C-RafpS259/fragment	2.00 Å	Sigma	Human	fragment	Ottmann, C. et al. (2010)[18]
3AXY	GF-14c/Hd3a/OsFD1	2.40 Å	Isoform c	Rice	-	Shimamoto, K. et al. (2011)[19]
3RDH	14-3-3ζ/FOBISIN101	2.40 Å	Zeta	Human	FOBISIN101	Fu, H. et al. (2011)[20]
3P1N	14-3-3σ/TASK3pS373	1.40 Å	Sigma	Human	-	Ottmann, C. et al. (2013)[21]
3P1O	14-3-3σ/TASK3pS373/FC-A	1.90 Å	Sigma	Human	Fusicoccin A	Ottmann, C. et al. (2013)[21]
3P1P	14-3-3σC38N_N166H/TASK3pS373	1.90 Å	Sigma	Human	-	Ottmann, C. et al. (2013)[21]
3P1Q	14-3-3σC38N_N166H/TASK3pS373/FC-A	1.70 Å	Sigma	Human	Fusicoccin A	Ottmann, C. et al. (2013)[21]
3P1R	14-3-3σC38V_N166H/TASK3pS373	1.70 Å	Sigma	Human	-	Ottmann, C. et al. (2013)[21]
3P1S	14-3-3σC38V_N166H/TASK3pS373/FC-A	1.65 Å	Sigma	Human	Fusicoccin A	Ottmann, C. et al. (2013)[21]
3UAL	14-3-3ε/MLF1pS34	1.80 Å	Epsilon	Human	-	Ottmann, C. et al. (2012)[22]
3UBW	14-3-3ε/MLF1pS34/fragment	1.90 Å	Epsilon	Human	fragment	Ottmann, C. et al. (2012)[22]
4DNK	14-3-3β	2.20 Å	Beta	Human	phosphate	-
3UZD	14-3-3γ/HDAC4pS350	1.86 Å	Gamma	Human	-	Min, J. et al. (2012)[23]
4E2E	14-3-3γ/HDAC4pS350	2.25 Å	Gamma	Human	-	-
3U9X	14-3-3σ/pyridoxalPD	1.80 Å	Sigma	Human	Pyridoxal-P-derivative	Ottmann, C. et al. (2012)[24]
4DX0	T14-3e/PMA2_CT30/pyrazole	3.40 Å	Isoform e	Tobacco	Pyrazole	Ottmann, C. et al. (2012)[25]
4DAT	14-3-3σ/PADI6pS446	1.40 Å	Sigma	Human	-	Ottmann, C. et al. (2012)[26]
4DAU	14-3-3σ/PADI6pS10	2.20 Å	Sigma	Human	-	Ottmann, C. et al. (2012)[26]
3SPR	14-3-3σC38V_N166H/TASK3pS373/FC-THF	1.99 Å	Sigma	Human	Fusicoccin THF	Ottmann, C. et al. (2013)[21]
3SMK	14-3-3σC38V_N166H/TASK3pS373/CN-A	2.10 Å	Sigma	Human	Cotylenin A	Ottmann, C. et al. (2013)[21]
3SML	14-3-3σC38N_N166H/TASK3pS373/FC-A aglycone	1.90 Å	Sigma	Human	Fusicoccin A aglycone	Ottmann, C. et al. (2013)[21]
3SMM	14-3-3σC38N_N166H/TASK3pS373/FC-J aglycone	2.00 Å	Sigma	Human	Fusicoccin J aglycone	Ottmann, C. et al. (2013)[21]

3SMN	14-3-3σC38N_N166H/TASK3pS373/FC THF	2.00 Å	Sigma	Human	Fusicoccin THF	Ottmann, C. et al. (2013)[21]
3SMO	14-3-3σC38V_N166H/TASK3pS373/FC-J aglycone	1.80 Å	Sigma	Human	Fusicoccin J aglycone	Ottmann, C. et al. (2013)[21]
3UX0	14-3-3σ/TASK3pS373/FC-H	1.75 Å	Sigma	Human	Fusicoccin H	Ottmann, C. et al. (2013)[21]
4FR3	14-3-3σ/TASK3pS373/FC-H derivative	1.90 Å	Sigma	Human	16-O-Me-Fusicoccin H	Ottmann, C. et al. (2013)[21]
3SP5	14-3-3σ/TASK3pS373/Cotylenol	1.80 Å	Sigma	Human	Cotylenol	Ottmann, C. et al. (2013)[21]
4FJ3	14-3-3ζ/C-RafpS233pS259	1.95 Å	Zeta	Human	-	Ottmann, C. et al. (2012)[27]
4GNT	14-3-3β/ChREBP	2.41 Å	Beta	Human	-	Uyeda, K. et al. (2012)[28]
3T0L	14-3-3σ/inhibitor	1.60 Å	Sigma	Human	Phosphonate B5	Ottmann, C. et al. (2013)[29]
3T0M	14-3-3σ/inhibitor	1.75 Å	Sigma	Human	Phosphonate B8	Ottmann, C. et al. (2013)[29]
4DHM	14-3-3σ/inhibitor	1.70 Å	Sigma	Human	Phosphonate B11	Ottmann, C. et al. (2013)[29]
4DHN	14-3-3σ/inhibitor	1.80 Å	Sigma	Human	Phosphonate B10	Ottmann, C. et al. (2013)[29]
4DHO	14-3-3σ/inhibitor	1.70 Å	Sigma	Human	Phosphonate B9	Ottmann, C. et al. (2013)[29]
4DHP	14-3-3σ/inhibitor	1.75 Å	Sigma	Human	Phosphonate B7	Ottmann, C. et al. (2013)[29]
4DHQ	14-3-3σ/inhibitor	1.75 Å	Sigma	Human	Phosphonate B6	Ottmann, C. et al. (2013)[29]
4DHR	14-3-3σ/inhibitor	1.40 Å	Sigma	Human	Phosphonate B4	Ottmann, C. et al. (2013)[29]
4DHS	14-3-3σ/inhibitor	1.74 Å	Sigma	Human	Phosphonate B3	Ottmann, C. et al. (2013)[29]
4DHT	14-3-3σ/inhibitor	1.80 Å	Sigma	Human	Phosphonate B2	Ottmann, C. et al. (2013)[29]
4DHU	14-3-3σ/inhibitor	1.67 Å	Sigma	Human	Phosphonate B1	Ottmann, C. et al. (2013)[29]
4HQW	14-3-3σ/molecular tweezer	2.35 Å	Sigma	Human	CLR01	Ottmann, C. et al. (2013)[30]
4HRU	14-3-3σ/molecular tweezer	3.15 Å	Sigma	Human	CLR01	Ottmann, C. et al. (2013)[30]
4JC3	14-3-3σ/ERαpT594	2.05 Å	Sigma	Human	-	Ottmann, C. et al. (2013)[31]
4JDD	14-3-3σ/ERαpT594/FC-A	2.10 Å	Sigma	Human	Fusicoccin A	Ottmann, C. et al. (2013)[31]
4F7R	g14-3-3	3.20 Å	-	Giardia intestinalis	Phosphate	Lalle, M. et al. (2014)[32]
4BG6	14-3-3ζ/Rnd3pS240	2.30 Å	Zeta	Human	-	Ridley, AJ. et al. (2013)[33]
4HKC	14-3-3ζ/α4pS1011	2.20 Å	Zeta	Human	-	Campbell, ID. et al. (2013)[34]

4IEA	14-3-3σ/C-RafpS629	1.70 Å	Sigma	Human	-	Ottmann, C. et al. (2013)[35]
4IHL	14-3-3ζ/C-RafpS233pS259/CN-A	2.20 Å	Zeta	Human	-	Ottmann, C. et al. (2013)[35]
4J6S	14-3-3γ/THpS19	3.08 Å	Gamma	Human	-	Martinez, A. et al. (2014)[36]
4FL5	14-3-3σ/TaupS214	1.90 Å	Sigma	Human	-	Ottmann, C. et al. (2015)[37]
5BTV	14-3-3σ/TaupS324	1.90 Å	Sigma	Human	-	Ottmann, C. et al. (2015)[37]
4N7G	14-3-3ζ/ExoS	2.25 Å	Zeta	Human	-	Ottmann, C. et al. (2014)[38]
4N7Y	14-3-3ζ/ExoSDerPep	2.16 Å	Zeta	Human	βRS8	Ottmann, C. et al. (2014)[38]
4N84	14-3-3ζ/ExoSDerPep	2.50 Å	Zeta	Human	βSS12	Ottmann, C. et al. (2014)[38]
4O46	14-3-3γ/NS1pS228	2.90 Å	Gamma	Human/Influenza		Min, J. et al. (2014)[39]
4WRQ	14-3-3ζ/ChibbypS20	2.41 Å	Zeta	Human	-	Choy et al. (2015)[40]
4QLI	14-3-3σ/SnailpT177	1.45 Å	Sigma	Human	-	-
4ZDR	14-3-3ζ/LKB1	2.90 Å	Zeta	Human	-	Zhu, Y. et al. (2015)[41]
4Y32	14-3-3σ/Tau109B	1.70 Å	Sigma	Human	Tau109B	Ottmann, C. et al. (2015)[42]
4Y3B	14-3-3σ/Tau201D	1.80 Å	Sigma	Human	Tau201D	Ottmann, C. et al. (2015)[42]
4Y5I	14-3-3σ/Tau126B	1.40 Å	Sigma	Human	Tau126B	Ottmann, C. et al. (2016)[42]
5D2D	14-3-3ζ/CFTRpS753pS768	2.10 Å	Zeta	Human	-	Ottmann, C. et al. (2016)[43]
5D3E	14-3-3γ/CFTRpS768pS795	2.75 Å	Gamma	Human	-	Ottmann, C. et al. (2016)[43]
5D3F	14-3-3ζ/CFTRpS753pS768/FC-A	2.74 Å	Zeta	Human	Fusicoccin A	Ottmann, C. et al. (2016)[43]
5F74	14-3-3β/ChREBP/AMP	2.35 Å	Beta	Human	Adenosine monophosphate	Uyeda, K. et al. (2012)[44]
5IQP	14-3-3τ	2.60 Å	Tau	Human	-	Gamblin, SJ. et al. (1995)[45]
AZQ0	g14-3-3/A8Ap	3.10 Å		Giardia intestinalis	-	Lalle, M. et al. (2015)[46]
5BY9	g14-3-3 polygly	4.00 Å		Giardia intestinalis	-	Lalle, M. et al. (2015)[46]
5EWZ	14-3-3ζ/Gab2pS210pT391	1.95 Å	Zeta	Human	-	Ottmann, C. et al. (2016)[47]
5EXA	14-3-3ζ/Gab2pT391/ISIR-005	1.70 Å	Zeta	Human	ISIR-005	Ottmann, C. et al. (2016)[47]
5J31	14-3-3ζ/ExoS derivative	2.40 Å	Zeta	Human/P.aeruginosa	Peptide H	Grossmann, TN. et al. (2016)[48]
5LTW	14-3-3σ/HSPB6	4.50 Å	Sigma	Human	-	Strelkov, SV. et al. (2017)[49]

5LU1	14-3-3σ/HSPB6pS16 (8mer)	2.40 Å	Sigma	Human	-	Strelkov, SV. et al. (2017)[49]
5LU2	14-3-3σ/HSPB6pS16 (13mer)	2.50 Å	Sigma	Human	-	Strelkov, SV. et al. (2017)[49]
5MY9	14-3-3σ/LRRK2pS935	1.33 Å	Sigma	Human	-	Ottmann, C. et al. (2017)[50]
5MYC	14-3-3σ/LRRK2pS910	1.46 Å	Sigma	Human	-	Ottmann, C. et al. (2017)[50]
5NAS	14-3-3ζ/PI4KIIIBpS294	2.08 Å	Zeta	Human	-	-
5LX2	LT 14-3-3/PI4KIIIBpS294	2.58 Å		La chancea thermotol erans	-	-
5WXN	14-3-3ζ/LKB1pT336	2.93 Å	Zeta	Human	-	Wu, J. et al. (2017)[51]
5JIT	14-3-3ζ/Cdc25pS216 (38mer)/CLR01	2.38 Å	Zeta	Human	CLR01	Ottmann, C. et al. (2017)[52]
5JIV	14-3-3ζ/Cdc25pS216 (38mer)/CLR01	2.45 Å	Zeta	Human	CLR01	Ottmann, C. et al. (2017)[52]
5JM4	14-3-3ζ/ExoS-adamantyl	2.34 Å	Zeta	Human	ExoS-adamantyl	Grossmann, T.N. et al. (2017)[53]
5N10	14-3-3ζ/FGG-ERβ/Q8	1.60 Å	Beta	Human	Cucubit[8]uril	Ottmann, C. et al. (2017)[54]
5N75	14-3-3σ/TAZpS89	1.80 Å	Sigma	Human	-	Ottmann, C. et al. (2017)[55]
5N5R	14-3-3σ/TAZpS89/NV1	1.80 Å	Sigma	Human	Fragment NV1	Ottmann, C. et al. (2017)[55]
5N5T	14-3-3σ/TAZpS89/NV2	1.80 Å	Sigma	Human	Fragment NV2	Ottmann, C. et al. (2017)[55]
5N5W	14-3-3σ/TAZpS89/NV2	1.37 Å	Sigma	Human	Fragment NV3	Ottmann, C. et al. (2017)[55]
5MOC	14-3-3σ/p53pT387	1.80 Å	Sigma	Human	-	Ottmann, C. et al. (2017)[56]
5MHC	14-3-3σ/p53pT387	1.20 Å	Sigma	Human	-	Ottmann, C. et al. (2017)[56]
5MXO	14-3-3σ/p53pT387/FC-A	1.20 Å	Sigma	Human	FC-A	Ottmann, C. et al. (2017)[56]
5OMA	14-3-3σ/StARD1pS57	3.90 Å	Sigma	Human	-	Sluchanko, N. et al., (2017)[57]
5OM0	14-3-3σ/Gli1pS640	3.20 Å	Sigma	Human	-	Sluchanko, N. et al., (2017)[57]
5OKF	14-3-3σ/HSPB6	3.20 Å	Sigma	Human	-	Sluchanko, N. et al., (2017)[57]
5OK9	14-3-3σ/HSPB6	2.35 Å	Sigma	Human	-	Sluchanko, N. et al., (2017)[57]
6EJL	14-3-3ζ/ASK1pS966	2.38 Å	Zeta	Human	-	-
6EWW	14-3-3ζ/CaMKK2pS100	2.70 Å	Zeta	Human	-	Obsil, T. et al. (2018)[58]
6FEL	14-3-3γ/CaMKK2pS511	2.84 Å	Gamma	Human	-	Obsil, T. et al. (2018)[58]
5NWK	14-3-3c/Kat1pS676/FC-A	3.30 Å	Isoform c	Nicotiana	FC-A	Moroni, A. et al. (2017)[59]

5NWJ	14-3-3c/Kat1pS676	2.07 Å	Isoform c	Nicotiana	-	Moroni, A. et al. (2017)[59]
5NWI	14-3-3c/Kat1pS676	2.35 Å	Isoform c	Nicotiana	-	Moroni, A. et al. (2017)[59]
5ULO	14-3-3ζ/TBC1D7pS124	2.14 Å	Zeta	Human	-	-
5YQG	14-3-3η/NumbpS265pS284	2.10 Å	Eta	Human	-	Wen, W. et al. (2018)[60]
6F08	14-3-3ζ/SOS1pS1161	1.90 Å	Zeta	Human	-	Ottmann, C. et al. (2018)[61]
6EIH	14-3-3ε/NELFEpS115	2.7 Å	Epsilon	Human	-	Beli, P. et al. (2018)[62]
6F09	14-3-3ζ/USP8pS718	1.59 Å	Zeta	Human	-	Ottmann, C. et al. (2018)[63]
6FCP	14-3-3σ/Shroom3P1244L	1.45 Å	Sigma	Human	-	Ottmann, C. et al. (2018)[64]
6FBB	14-3-3σ/Shroom3WT	1.30 Å	Sigma	Human	-	Ottmann, C. et al. (2018)[64]
6BZD	14-3-3γR57E/GlcNacPep	2.67 Å	Gamma	Human	-	Boyce, M. et al. (2018)[65]
6BYL	14-3-3γ/GlcNacPep	3.35 Å	Gamma	Human	-	Boyce, M. et al. (2018)[65]
6BYK	14-3-3β/GlcNacPep	3.00 Å	Beta	Human	-	Boyce, M. et al. (2018)[65]
6BYJ	14-3-3γ/GlcNacPep	2.90 Å	Gamma	Human	-	Boyce, M. et al. (2018)[65]
6FI5	14-3-3σ/TauDeriv3.2	1.70 Å	Sigma	Human	-	Ottmann, C. et al. (2018)[66]
6FI4	14-3-3σ/TauDeriv3.2e	2.00 Å	Sigma	Human	-	Ottmann, C. et al. (2018)[66]
6FBY	14-3-3σ/TauDeriv4.2b	1.50 Å	Sigma	Human	-	Ottmann, C. et al. (2018)[66]
6FBW	14-3-3σ/TauDeriv4.2f-II	1.45 Å	Sigma	Human	-	Ottmann, C. et al. (2018)[66]
6FAW	14-3-3σ/TauDeriv4.2c-I	1.40 Å	Sigma	Human	-	Ottmann, C. et al. (2018)[66]
6FAV	14-3-3σ/TauDeriv4.2f-I	1.40 Å	Sigma	Human	-	Ottmann, C. et al. (2018)[66]
6FAU	14-3-3σ/TauDeriv4.2e-I	1.25 Å	Sigma	Human	-	Ottmann, C. et al. (2018)[66]
5WFX	14-3-3β/Malate	1.65 Å	Beta	Human	Malate	-
6FNC	14-3-3ζ/Biv1	2.12 Å	Zeta	Human	-	Ottmann, C. et al. (2018)[67]
6FNA	14-3-3ζ/Biv2	2.12 Å	Zeta	Human	-	Ottmann, C. et al. (2018)[67]
6FNB	14-3-3ζ/Biv3	2.30 Å	Zeta	Human	-	Ottmann, C. et al. (2018)[67]
6FN9	14-3-3ζ/Mov2	2.27 Å	Zeta	Human	-	Ottmann, C. et al. (2018)[67]
5XY9	14-3-3ζ/MST4	2.30 Å	Zeta	Human	-	-
5WFU	14-3-3β/Malate	1.97 Å	Beta	Human	Malate	-
6GHP	14-3-3σ/TASK3/FCNac	1.95 Å	Sigma	Human	FC-NAc	Ottmann, C. et al. (2018)[68]

6GNN	14-3-3β/ExoT	3.79 Å	Beta	Human	-	Schueler, H. et al. (2018)[69]
6GNK	14-3-3β/ExoS	2.55 Å	Beta	Human	-	Schueler, H. et al. (2018)[69]
6GNJ	14-3-3β/ExoS	3.24 Å	Beta	Human	-	Schueler, H. et al. (2018)[69]
6GN8	14-3-3β/ExoS	2.34 Å	Beta	Human	-	Schueler, H. et al. (2018)[69]
6GN0	14-3-3β/ExoS	3.24 Å	Beta	Human	-	Schueler, H. et al. (2018)[69]
6GKG	14-3-3γ/Casp2pS164	2.85 Å	Gamma	Human	-	Obsilova, V. et al. (2018)[70]
6GKF	14-3-3γ/Casp2pS139	2.60 Å	Gamma	Human	-	Obsilova, V. et al. (2018)[70]
6HEP	14-3-3β/CFTRpS753pS768	1.86Å	Beta	Human	-	Ottmann, C. et al. (2018)[71]
6BD2	14-3-3θ/IRSp53pT340pS366	2.90Å	Theta	Human	-	-
6BD1	14-3-3θ/IRSp53pS366	2.35Å	Theta	Human	-	-
6BCY	14-3-3θ/IRSp53pS360	2.30Å	Theta	Human	-	-
6BCR	14-3-3θ/IRSp53pS340	1.99Å	Theta	Human	-	-

Table S1 References

1. Petosa C, Masters SC, Bankston LA, Pohl J, Wang B, Fu H, Liddington RC. 14-3-3zeta binds a phosphorylated Raf peptide and an unphosphorylated peptide via its conserved amphipathic groove. J Biol Chem. 1998 Jun 26;273(26):16305-10.

2. Liu D, Bienkowska J, Petosa C, Collier RJ, Fu H, Liddington R. Crystal structure of the zeta isoform of the 14-3-3 protein. Nature. 1995 Jul 13;376(6536):191-4.

3. Rittinger K, Budman J, Xu J, Volinia S, Cantley LC, Smerdon SJ, Gamblin SJ, Yaffe MB. Structural analysis of 14-3-3 phosphopeptide complexes identifies a dual role for the nuclear export signal of 14-3-3 in ligand binding. Mol Cell. 1999 Aug;4(2):153-66.

4. Obsil T, Ghirlando R, Klein DC, Ganguly S, Dyda F. Crystal structure of the 14-3-3zeta:serotonin N-acetyltransferase complex. a role for scaffolding in enzyme regulation. Cell. 2001 Apr 20;105(2):257-67.

5. Würtele M, Jelich-Ottmann C, Wittinghofer A, Oecking C. Structural view of a fungal toxin acting on a 14-3-3 regulatory complex. EMBO J. 2003 Mar 3;22(5):987-94.

6. Wilker EW, Grant RA, Artim SC, Yaffe MB. A structural basis for 14-3-3sigma functional specificity. J Biol Chem. 2005 May 13;280(19):18891-8.

7. Benzinger A, Popowicz GM, Joy JK, Majumdar S, Holak TA, Hermeking H. The crystal structure of the non-liganded 14-3-3sigma protein: insights into determinants of isoform specific ligand binding and dimerization.

8. Yang X, Lee WH, Sobott F, Papagrigoriou E, Robinson CV, Grossmann JG, Sundström M, Doyle DA, Elkins JM. Structural basis for protein-protein interactions in the 14-3-3 protein family. Proc Natl Acad Sci U S A. 2006 Nov 14;103(46):17237-42.

9. Macdonald N, Welburn JP, Noble ME, Nguyen A, Yaffe MB, Clynes D, Moggs JG, Orphanides G, Thomson S, Edmunds JW, Clayton AL, Endicott JA, Mahadevan LC. Molecular basis for the recognition of phosphorylated and phosphoacetylated histone h3 by 14-3-3. Mol Cell. 2005 Oct 28;20(2):199-211.

10. Brokx SJ, Wernimont AK, Dong A, Wasney GA, Lin YH, Lew J, Vedadi M, Lee WH, Hui R. Characterization of 14-3-3 proteins from Cryptosporidium parvum. PLoS One. 2011;6(8):e14827

11. Ottmann C, Marco S, Jaspert N, Marcon C, Schauer N, Weyand M, Vandermeeren C, Duby G, Boutry M, Wittinghofer A, Rigaud JL, Oecking C. Structure of a 14-3-3 coordinated hexamer of the plant plasma membrane H+ -ATPase by combining X-ray crystallography and electron cryomicroscopy. Mol Cell. 2007 Feb 9;25(3):427-40.

12. Ottmann C, Yasmin L, Weyand M, Veesenmeyer JL, Diaz MH, Palmer RH, Francis MS, Hauser AR, Wittinghofer A, Hallberg B. Phosphorylation-independent interaction between 14-3-3 and exoenzyme S: from structure to pathogenesis. EMBO J. 2007 Feb 7;26(3):902-13.

13. Takala H, Nurminen E, Nurmi SM, Aatonen M, Strandin T, Takatalo M, Kiema T, Gahmberg CG, Ylänne J, Fagerholm SC. Beta2 integrin phosphorylation on Thr758 acts as a molecular switch to regulate 14-3-3 and filamin binding. Blood. 2008 Sep 1;112(5):1853-62.

14. Ottmann C, Weyand M, Sassa T, Inoue T, Kato N, Wittinghofer A, Oecking C. A structural rationale for selective stabilization of anti-tumor interactions of 14-3-3 proteins by cotylenin A. J Mol Biol. 2009 Mar 6;386(4):913-9.

15. Molzan M, Schumacher B, Ottmann C, Baljuls A, Polzien L, Weyand M, Thiel P, Rose R, Rose M, Kuhenne P, Kaiser M, Rapp UR, Kuhlmann J, Ottmann C. Impaired binding of 14-3-3 to C-RAF in Noonan syndrome suggests new approaches in diseases with increased Ras signaling. Mol Cell Biol. 2010 Oct;30(19):4698-711.

16. Kostelecky B, Saurin AT, Purkiss A, Parker PJ, McDonald NQ. Recognition of an intra-chain tandem 14-3-3 binding site within PKCepsilon. EMBO Rep. 2009 Sep;10(9):983-9.

17. Schumacher B, Skwarczynska M, Rose R, Ottmann C. Structure of a 14-3-3σ-YAP phosphopeptide complex at 1.15 A resolution. Acta Crystallogr Sect F Struct Biol Cryst Commun. 2010 Sep 1;66(Pt 9):978-84.

18. Molzan M, Schumacher B, Ottmann C, Baljuls A, Polzien L, Weyand M, Thiel P, Rose R, Rose M, Kuhenne P, Kaiser M, Rapp UR, Kuhlmann J, Ottmann C. Impaired binding of 14-3-3 to C-RAF in Noonan syndrome suggests new approaches in diseases with increased Ras signaling. Mol Cell Biol. 2010 Oct;30(19):4698-711.

19. Taoka K, Ohki I, Tsuji H, Furuita K, Hayashi K, Yanase T, Yamaguchi M, Nakashima C, Purwestri YA, Tamaki S, Ogaki Y, Shimada C, Nakagawa A, Kojima C, Shimamoto K. 14-3-3 proteins act as intracellular receptors for rice Hd3a florigen. Nature. 2011 Jul 31;476(7360):332-5.

20. Zhao J, Du Y, Horton JR, Upadhyay AK, Lou B, Bai Y, Zhang X, Du L, Li M, Wang B, Zhang L, Barbieri JT, Khuri FR, Cheng X, Fu H. Discovery and structural characterization of a small molecule 14-3-3 protein-protein interaction inhibitor. Proc Natl Acad Sci U S A. 2011 Sep 27;108(39):16212-6.

21. Anders C, Higuchi Y, Koschinsky K, Bartel M, Schumacher B, Thiel P, Nitta H, Preisig-Müller R, Schlichthörl G, Renigunta V, Ohkanda J, Daut J, Kato N, Ottmann C. A semisynthetic fusicoccane stabilizes a protein-protein interaction and enhances the expression of K+ channels at the cell surface. Chem Biol. 2013 Apr 18;20(4):583-93.

22. Molzan M, Weyand M, Rose R, Ottmann C. Structural insights of the MLF1/14-3-3 interaction. FEBS J. 2012 Feb;279(4):563-71.

23. Xu C, Jin J, Bian C, Lam R, Tian R, Weist R, You L, Nie J, Bochkarev A, Tempel W, Tan CS, Wasney GA, Vedadi M, Gish GD, Arrowsmith CH, Pawson T, Yang XJ, Min J Sequence-specific recognition of a PxLPxI/L motif by an ankyrin repeat tumbler lock. Sci Signal. 2012 May 29;5(226):ra39.

24. Röglin L, Thiel P, Kohlbacher O, Ottmann C. Covalent attachment of pyridoxal-phosphate derivatives to 14-3-3 proteins. Proc Natl Acad Sci U S A. 2012 May 1;109(18):E1051-3

25. Richter A, Rose R, Hedberg C, Waldmann H, Ottmann C. An optimised small-molecule stabiliser of the 14-3-3-PMA2 protein-protein interaction. Chemistry. 2012 May 21;18(21):6520-7.

26. Rose R, Rose M, Ottmann C. Identification and structural characterization of two 14-3-3 binding sites in the human peptidylarginine deiminase type VI. J Struct Biol. 2012 Oct;180(1):65-72.

27. Molzan M, Ottmann C. Synergistic binding of the phosphorylated S233- and S259-binding sites of C-RAF to one 14-3-3ζ dimer. J Mol Biol. 2012 Nov 2;423(4):486-95.

28. Ge Q, Huang N, Wynn RM, Li Y, Du X, Miller B, Zhang H, Uyeda K. Structural characterization of a unique interface between carbohydrate response element-binding protein (ChREBP) and 14-3-3β protein. J Biol Chem. 2012 Dec 7;287(50):41914-21.

29. Thiel P, Röglin L, Meissner N, Hennig S, Kohlbacher O, Ottmann C. Virtual screening and experimental validation reveal novel small-molecule inhibitors of 14-3-3 protein-protein interactions. Chem Commun (Camb). 2013 Oct 4;49(76):8468-70.

30. Bier D, Rose R, Bravo-Rodriguez K, Bartel M, Ramirez-Anguita JM, Dutt S, Wilch C, Klärner FG, Sanchez-Garcia E, Schrader T, Ottmann C. Molecular tweezers modulate 14-3-3 protein-protein interactions. Nat Chem. 2013 Mar;5(3):234-9.

31. De Vries-van Leeuwen IJ, da Costa Pereira D, Flach KD, Piersma SR, Haase C, Bier D, Yalcin Z, Michalides R, Feenstra KA, Jiménez CR, de Greef TF, Brunsveld L, Ottmann C, Zwart W, de Boer AH. Interaction of 14-3-3 proteins with the estrogen receptor alpha F domain provides a drug target interface. Proc Natl Acad Sci U S A. 2013 May 28;110(22):8894-9.

32. Fiorillo A, di Marino D, Bertuccini L, Via A, Pozio E, Camerini S, Ilari A, Lalle M. The crystal structure of Giardia duodenalis 14-3-3 in the apo form: when protein post-translational modifications make the difference. PLoS One. 2014 Mar 21;9(3):e92902.

33. Riou P, Kjær S, Garg R, Purkiss A, George R, Cain RJ, Bineva G, Reymond N, McColl B, Thompson AJ, O'Reilly N, McDonald NQ, Parker PJ, Ridley AJ. 14-3-3 proteins interact with a hybrid prenyl-phosphorylation motif to inhibit G proteins. Cell. 2013 Apr 25;153(3):640-53.

34. Bonet R, Vakonakis I, Campbell ID. Characterization of 14-3-3-ζ Interactions with integrin tails. J Mol Biol. 2013 Sep 9;425(17):3060-72.

35. Molzan M, Kasper S, Röglin L, Skwarczynska M, Sassa T, Inoue T, Breitenbuecher F, Ohkanda J, Kato N, Schuler M, Ottmann C. Stabilization of physical RAF/14-3-3 interaction by cotylenin A as treatment strategy for RAS mutant cancers. ACS Chem Biol. 2013 Sep 20;8(9):1869-75.

36. Skjevik AA, Mileni M, Baumann A, Halskau O, Teigen K, Stevens RC, Martinez A. The N-terminal sequence of tyrosine hydroxylase is a conformationally versatile motif that binds 14-3-3 proteins and membranes. J Mol Biol. 2014 Jan 9;426(1):150-68.

37. Joo Y, Schumacher B, Landrieu I, Bartel M, Smet-Nocca C, Jang A, Choi HS, Jeon NL, Chang KA, Kim HS, Ottmann C, Suh YH. Involvement of 14-3-3 in tubulin instability and impaired axon development is mediated by Tau. FASEB J. 2015 Oct;29(10):4133-44.

38. Glas A, Bier D, Hahne G, Rademacher C, Ottmann C, Grossmann TN. Constrained peptides with target-adapted cross-links as inhibitors of a pathogenic protein-protein interaction. Angew Chem Int Ed Engl. 2014 Feb 24;53(9):2489-93.

39. Qin S, Liu Y, Tempel W, Eram MS, Bian C, Liu K, Senisterra G, Crombet L, Vedadi M, Min J. Structural basis for histone mimicry and hijacking of host proteins by influenza virus protein NS1. Nat Commun. 2014 May 23;5:3952

40. Killoran RC, Fan J, Yang D, Shilton BH, Choy WY. Structural Analysis of the 14-3-3ζ/Chibby Interaction Involved in Wnt/β-Catenin Signaling. PLoS One. 2015 Apr 24;10(4):e0123934.

41. Ding S, Zhou R, Zhu Y. Structure of the 14-3-3ζ-LKB1 fusion protein provides insight into a novel ligand-binding mode of 14-3-3. Acta Crystallogr F Struct Biol Commun. 2015 Sep;71(Pt 9):1114-9.

42. Milroy LG, Bartel M, Henen MA, Leysen S, Adriaans JM, Brunsveld L, Landrieu I, Ottmann C. Stabilizer-Guided Inhibition of Protein-Protein Interactions. Angew Chem Int Ed Engl. 2015 Dec 21;54(52):15720-4.

43. Stevers LM, Lam CV, Leysen SF, Meijer FA, van Scheppingen DS, de Vries RM, Carlile GW, Milroy LG, Thomas DY, Brunsveld L, Ottmann C. Characterization and small-molecule stabilization of the multisite tandem binding between 14-3-3 and the R domain of CFTR. Proc Natl Acad Sci U S A. 2016 Mar 1;113(9):E1152-61.

44. Sato S, Jung H, Nakagawa T, Pawlosky R, Takeshima T, Lee WR, Sakiyama H, Laxman S, Wynn RM, Tu BP, MacMillan JB, De Brabander JK, Veech RL, Uyeda K. Metabolite Regulation of Nuclear Localization of Carbohydrate-response Element-binding Protein (ChREBP): ROLE OF AMP AS AN ALLOSTERIC INHIBITOR. J Biol Chem. 2016 May 13;291(20):10515-27.

45. Xiao B, Smerdon SJ, Jones DH, Dodson GG, Soneji Y, Aitken A, Gamblin SJ. Structure of a 14-3-3 protein and implications for coordination of multiple signalling pathways. Nature. 1995 Jul 13;376(6536):188-91.

46. Cau Y, Fiorillo A, Mori M, Ilari A, Botta M, Lalle M. Molecular Dynamics Simulations and Structural Analysis of Giardia duodenalis 14-3-3 Protein-Protein Interactions. J Chem Inf Model. 2015 Dec 28;55(12):2611-22.

47. Bier D, Bartel M, Sies K, Halbach S, Higuchi Y, Haranosono Y, Brummer T, Kato N, Ottmann C. Small-Molecule Stabilization of the 14-3-3/Gab2 Protein-Protein Interaction (PPI) Interface. ChemMedChem. 2016 Apr 19;11(8):911-8.

48. Cromm PM, Wallraven K, Glas A, Bier D, Fürstner A, Ottmann C, Grossmann TN. Constraining an Irregular Peptide Secondary Structure through Ring-Closing Alkyne Metathesis. Chembiochem. 2016 Oct 17;17(20):1915-1919.

49. Sluchanko NN, Beelen S, Kulikova AA, Weeks SD, Antson AA, Gusev NB, Strelkov SV. Structural Basis for the Interaction of a Human Small Heat Shock Protein with the 14-3-3 Universal Signaling Regulator. Structure. 2017 Feb 7;25(2):305-316.

50. Stevers LM, de Vries RM, Doveston RG, Milroy LG, Brunsveld L, Ottmann C. Structural interface between LRRK2 and 14-3-3 protein. Biochem J. 2017 Mar 23;474(7):1273-1287.

51. Lu Y, Ding S, Zhou R, Wu J. Structure of the complex of phosphorylated liver kinase B1 and 14-3-3ζ. Acta Crystallogr F Struct Biol Commun. 2017 Apr 1;73(Pt 4):196-201.

52. Bier D, Mittal S, Bravo-Rodriguez K, Sowislok A, Guillory X, Briels J, Heid C, Bartel M, Wettig B, Brunsveld L, Sanchez-Garcia E, Schrader T, Ottmann C. The Molecular Tweezer CLR01 Stabilizes a Disordered Protein-Protein Interface. J Am Chem Soc. 2017 Nov 15;139(45):16256-16263.

53. de Vink PJ, Briels JM, Schrader T, Milroy LG, Brunsveld L, Ottmann C. A Binary Bivalent Supramolecular Assembly Platform Based on Cucurbit[8]uril and Dimeric Adapter Protein 14-3-3. Angew Chem Int Ed Engl. 2017 May 16.

54. Krüger DM, Glas A, Bier D, Pospiech N, Wallraven K, Dietrich L, Ottmann C, Koch O, Hennig S, Grossmann TN. Structure-Based Design of Non-natural Macrocyclic Peptides That Inhibit Protein-Protein Interactions. J Med Chem. 2017 Nov 9;60(21):8982-8988.

55. Sijbesma E, Skora L, Leysen S, Brunsveld L, Koch U, Nussbaumer P, Jahnke W, Ottmann C. Identification of two secondary ligand binding sites in 14-3-3 proteins using fragment screening. Biochemistry. 2017 Jul 6. doi: 10.1021/acs.biochem.7b00153.

56. Doveston RG, Kuusk A, Andrei SA, Leysen S, Cao Q, Castaldi MP, Hendricks A, Brunsveld L, Chen H, Boyd H, Ottmann C. Small-molecule stabilization of the p53 - 14-3-3 protein-protein interaction. FEBS Lett. 2017 Aug;591(16):2449-2457.

57. Sluchanko NN, Tugaeva KV, Greive SJ, Antson AA. Chimeric 14-3-3 proteins for unraveling interactions with intrinsically disordered partners. Sci Rep. 2017 Sep 20;7(1):12014.

58. Psenakova K, Petrvalska O, Kylarova S, Lentini Santo D, Kalabova D, Herman P, Obsilova V, Obsil T. 14-3-3 protein directly interacts with the kinase domain of calcium/calmodulin-dependent protein kinase kinase (CaMKK2). Biochim Biophys Acta Gen Subj. 2018 Jul;1862(7):1612-1625.

59. Saponaro A, Porro A, Chaves-Sanjuan A, Nardini M, Rauh O, Thiel G, Moroni A. Fusicoccin Activates KAT1 Channels by Stabilizing Their Interaction with 14-3-3 Proteins. Plant Cell. 2017 Oct;29(10):2570-2580.

60. Chen X, Liu Z, Shan Z, Yao W, Gu A, Wen W. Structural determinants controlling 14-3-3 recruitment to the endocytic adaptor Numb and dissociation of the Numb·α-adaptin complex. J Biol Chem. 2018 Mar 16;293(11):4149-4158.

61. Ballone A, Centorrino F, Wolter M, Ottmann C. Structural characterization of 14-3-3ζ in complex with the human Son of sevenless homolog 1 (SOS1). J Struct Biol. 2018 Jun;202(3):210-215.

62. Borisova ME, Voigt A, Tollenaere MAX, Sahu SK, Juretschke T, Kreim N, Mailand N, Choudhary C, Bekker-Jensen S, Akutsu M, Wagner SA, Beli P. p38-MK2 signaling axis regulates RNA metabolism after UV-light-induced DNA damage. Nat Commun. 2018 Mar 9;9(1):1017.

63. Centorrino F, Ballone A, Wolter M, Ottmann C. Biophysical and structural insight into the USP8/14-3-3 interaction. FEBS Lett. 2018 Apr;592(7):1211-1220.

64. Prokop JW, Yeo NC, Ottmann C, Chhetri SB, Florus KL, Ross EJ, Sosonkina N, Link BA, Freedman BI, Coppola CJ, McDermott-Roe C, Leysen S, Milroy LG, Meijer FA, Geurts AM, Rauscher FJ 3rd, Ramaker R, Flister MJ, Jacob HJ, Mendenhall EM, Lazar J. Characterization of Coding/Noncoding Variants for SHROOM3 in Patients with CKD. J Am Soc Nephrol. 2018 May;29(5):1525-1535.

65. Toleman CA, Schumacher MA, Yu SH, Zeng W, Cox NJ, Smith TJ, Soderblom EJ, Wands AM, Kohler JJ, Boyce M. Structural basis of O-GlcNAc recognition by mammalian 14-3-3 proteins. Proc Natl Acad Sci U S A. 2018 Jun 5;115(23):5956-5961.

66. Andrei SA, Meijer FA, Neves JF, Brunsveld L, Landrieu I, Ottmann C, Milroy LG. Inhibition of 14-3-3/Tau by Hybrid Small-Molecule Peptides Operating via Two Different Binding Modes. ACS Chem Neurosci. 2018 May 17. doi: 10.1021/acschemneuro.8b00118.

67. Yilmaz E, Bier D, Guillory X, Briels J, Ruiz-Blanco YB, Sanchez-Garcia E, Ottmann C, Kaiser M. Mono- and Bivalent 14-3-3 Inhibitors for Characterizing Supramolecular "Lysine Wrapping" of Oligoethylene Glycol (OEG) Moieties in Proteins. Chemistry. 2018 Sep 18;24(52):13807-13814.

68. Andrei SA, de Vink P, Sijbesma E, Han L, Brunsveld L, Kato N, Ottmann C, Higuchi Y. Rationally Designed Semisynthetic Natural Product Analogues for Stabilization of 14-3-3 Protein-Protein Interactions. Angew Chem Int Ed Engl. 2018 Oct 8;57(41):13470-13474.

69. Karlberg T, Hornyak P, Pinto AF, Milanova S, Ebrahimi M, Lindberg M, Püllen N, Nordström A, Löverli E, Caraballo R, Wong EV, Näreoja K, Thorsell AG, Elofsson M, De La Cruz EM, Björkegren C, Schüler H. 14-3-3 proteins activate Pseudomonas exotoxins-S and -T by chaperoning a hydrophobic surface. Nat Commun. 2018 Sep 17;9(1):3785.

70. Smidova A, Alblova M, Kalabova D, Psenakova K, Rosulek M, Herman P, Obsil T, Obsilova V. 14-3-3 protein masks the nuclear localization sequence of caspase-2. FEBS J. 2018 Oct 3. doi: 10.1111/febs.14670.

71. Stevers LM, de Vink PJ, Ottmann C, Huskens J, Brunsveld L. A Thermodynamic Model for Multivalency in 14-3-3 Protein-Protein Interactions. J Am Chem Soc. 2018 Oct 18. doi: 10.1021/jacs.8b09618

8. References

1S. Pronk, S. Páll, R. Schulz, P. Larsson, P. Bjelkmar, R. Apostolov, M. R. Shirts, J. C. Smith, P. M. Kasson, D. van der Spoel, B. Hess and E. Lindahl, *Bioinformatics*, 2013, **29**, 845–854.

2J.-N. Grad, A. Gigante, C. Wilms, J. N. Dybowski, L. Ohl, C. Ottmann, C. Schmuck and D. Hoffmann, *J Chem Inf Model*, 2018, **58**, 315–327.

3Q.-Q. Jiang, W. Sicking, M. Ehlers and C. Schmuck, *Chem Sci*, 2015, **6**, 1792–1800.